Probing signals of compressed spectra in Supersymmetry at LHC

Juhi Dutta

University of Hamburg

March 2, 2020

Based on JHEP 01 (2016) 051, JHEP 09 (2017) 026, JHEP 06 (2018) 042
with A.Chatterjee, P. Konar, S. Mondal, B. Mukhopadhyaya, S.K. Rai

Outline

- SUSY as a BSM theory
- Compressed spectra in SUSY
  - with $\widetilde{\chi}_1^0$ LSP.
  - with $\widetilde{G}$ LSP.
  - with $\widetilde{\nu}_R$ LSP.
- Results and Conclusions

SUSY as a BSM theory

- Supersymmetry(SUSY) is one of the well motivated candidates for Beyond Standard Model (BSM) Physics.
- It is a symmetry connecting fermions and bosons.
- Introduces a superpartner differing by spin $\frac{1}{2}$ for every Standard Model (SM) particle.
- R-parity conserving SUSY provides a stable, neutral dark matter candidate, mostly $\widetilde{\chi}_1^0$.

Particle Content of SUSY

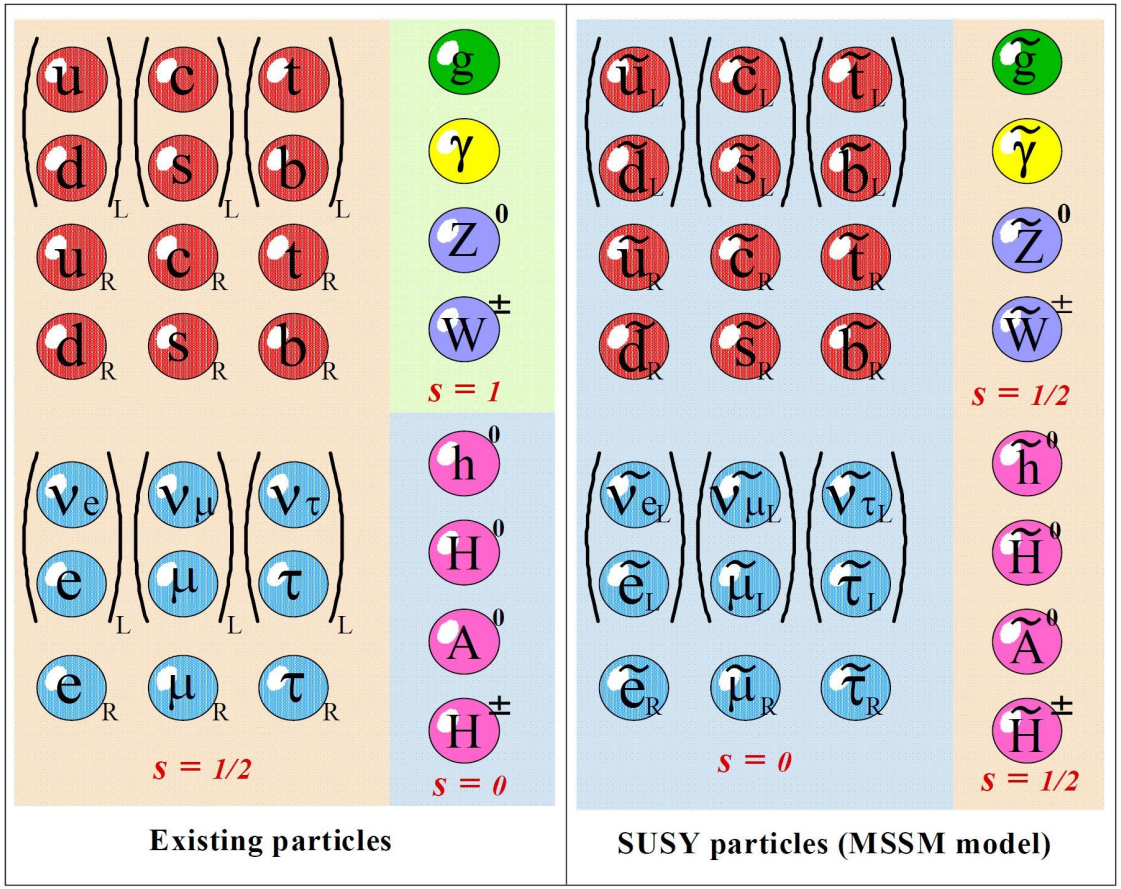

Motivation

- Conventional SUSY scenarios: mSUGRA, GMSB $\Longrightarrow$ universal SUSY breaking with few free parameters

- Conventional signals for SUSY: hard jets/leptons + $\not{E}_T$ looked for extensively at LHC.

Current status of SUSY

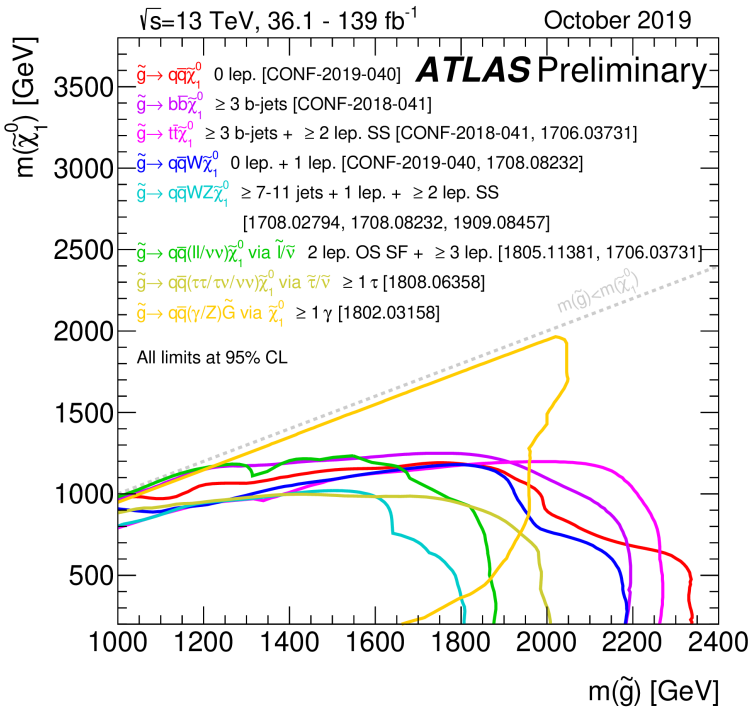

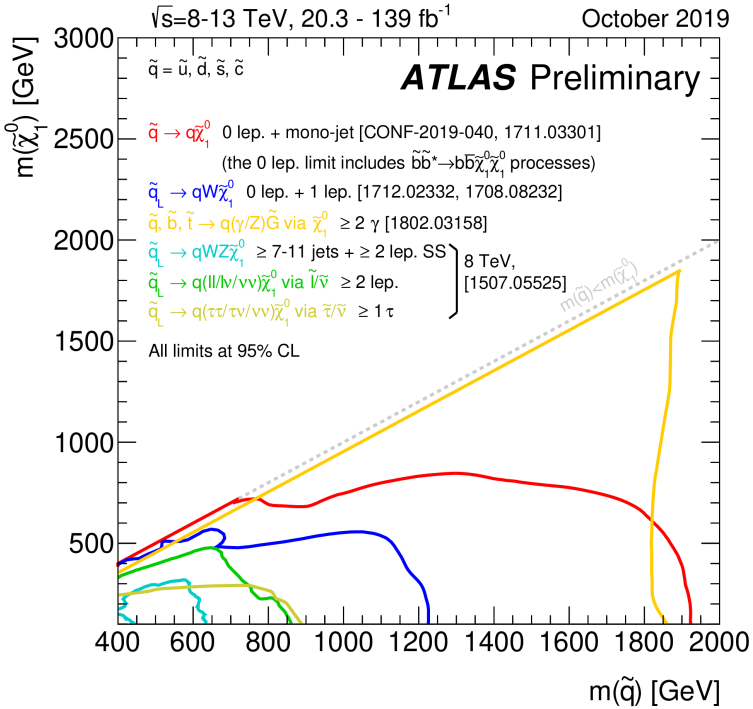

Current status of SUSY

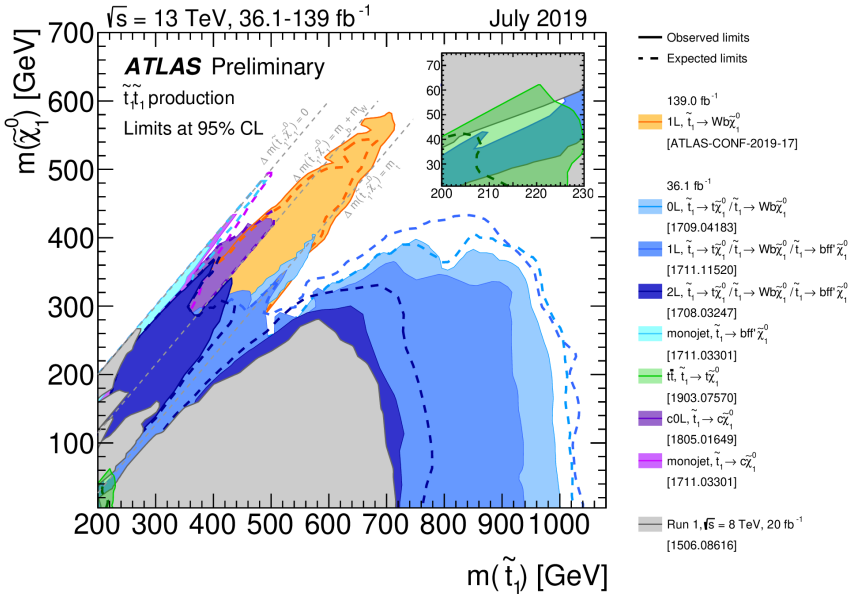

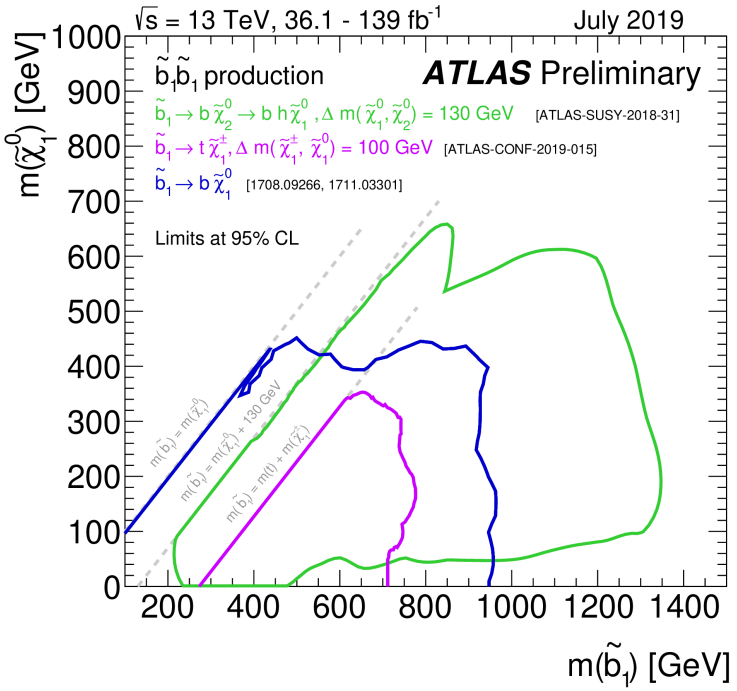

- No hints of Beyond Standard Model Physics yet observed.

- *Where is SUSY hiding?*

Possibilities

- SUSY spectra could be heavy $\Longrightarrow$ beyond current experimental reach.

- SUSY is invisible from current search strategies at LHC.

- Searches mostly geared towards observing conventional SUSY signals $\Longrightarrow$ with triggers on hard objects (leptons, (b)-jets, photons, missing transverse energy ($\not{E}_T$).

- Thus, objects with low p_T remain invisible to such triggers $\Longrightarrow$ *compressed spectra*, unless there are additional hard objects to trigger upon.

- Further, signal selection criteria often are not sensitive to soft objects .

- Tremendous experimental efforts to improve detection of soft objects (1911.12606).

Compressed spectra

- Compressed spectra have relatively closely spaced sparticles.
- Such a spectrum produces soft jets, leptons and missing transverse energy $\rightarrow$ may not pass the signal selection criterions leading to weak bounds on such spectra.

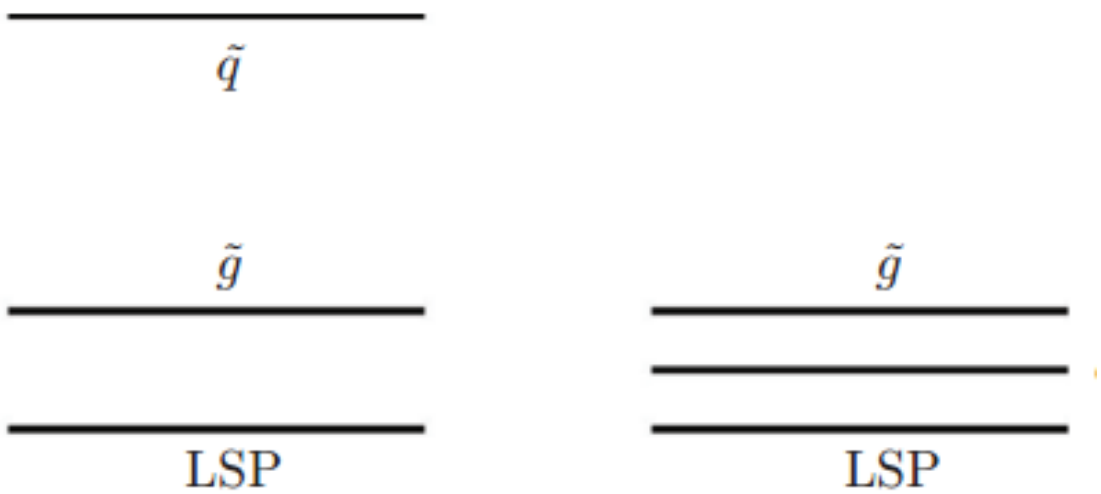

(T. J. LeCompte, S. P. Martin, Phys.Rev. D84 (2011) 015004, Dreiner, et.al, 2012 EPL 99 61001)

- Most studies in this direction focus on simplified models with a squark or gluino NLSP compressed with the LSP.
- Rest of the spectrum inconsequential.
- Monojet + $\not{E}_T \rightarrow$ trademark channel for discovery.

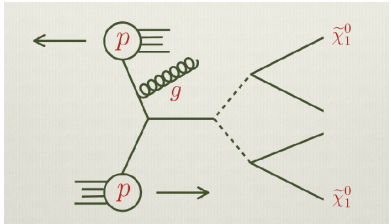

- Much more appropriate event selection criteria for observing multiple jets and missing energy signals emphasising on tails of distributions.
(B.Bhattacharjee et.al, Phys Rev. D89 (2014) no.3, 037702, G.Chalons, D.Sengupta JHEP 1512 (2015) 129).

- Theoretical efforts to use soft tracks in addition to mono-jet to improve signal (S.Chakraborty et.al, PRD 94(2016)no.11,111703)

- Such a compressed spectra also yields the thermal relic density for the DM candidate due to the presence of coannihilation partners.

Overview of work done

- We explore compressed spectra in the context of MSSM and its extensions.
- Effect of relevant constraints on the spectra
- Signals at LHC
- Attempt to distinguish uncompressed and compressed scenarios

Case I: Compression in MSSM

Non-universal SUSY breaking at high scale could give rise to a compressed spectrum with masses of gluinos, squarks, sleptons close to the $\widetilde{\chi}_1^0$ LSP.

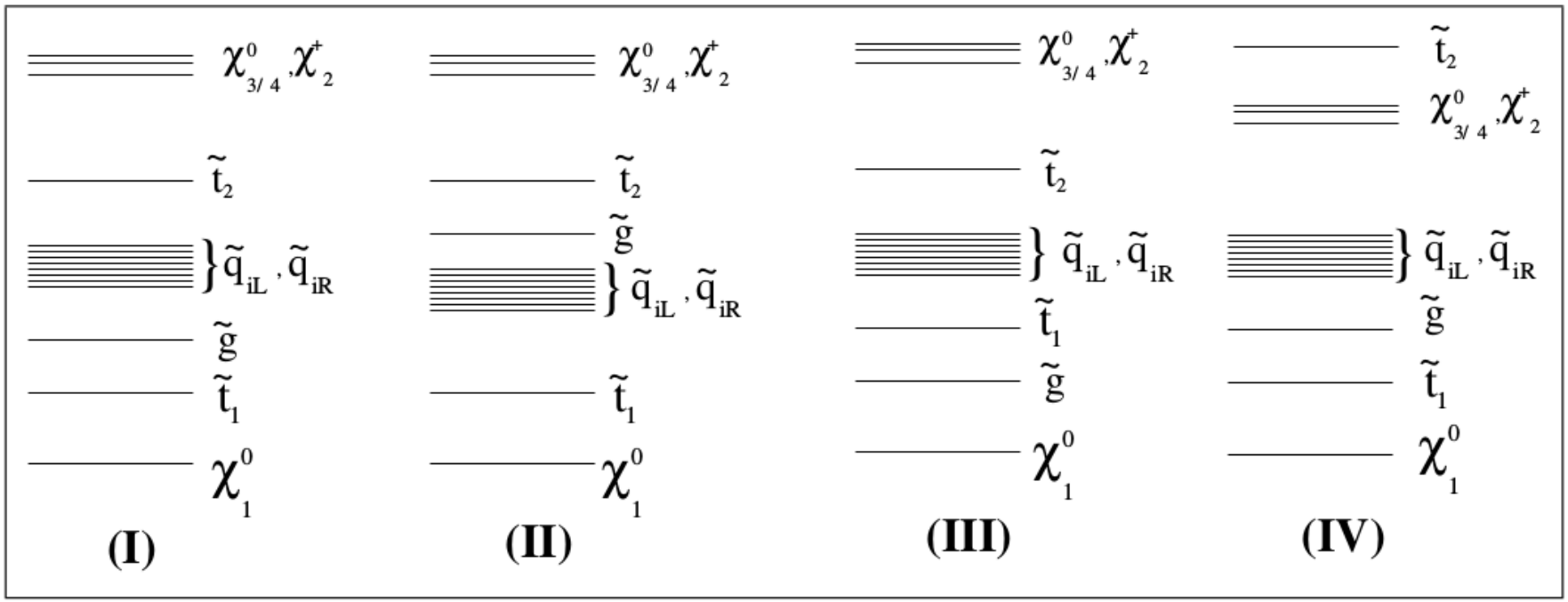

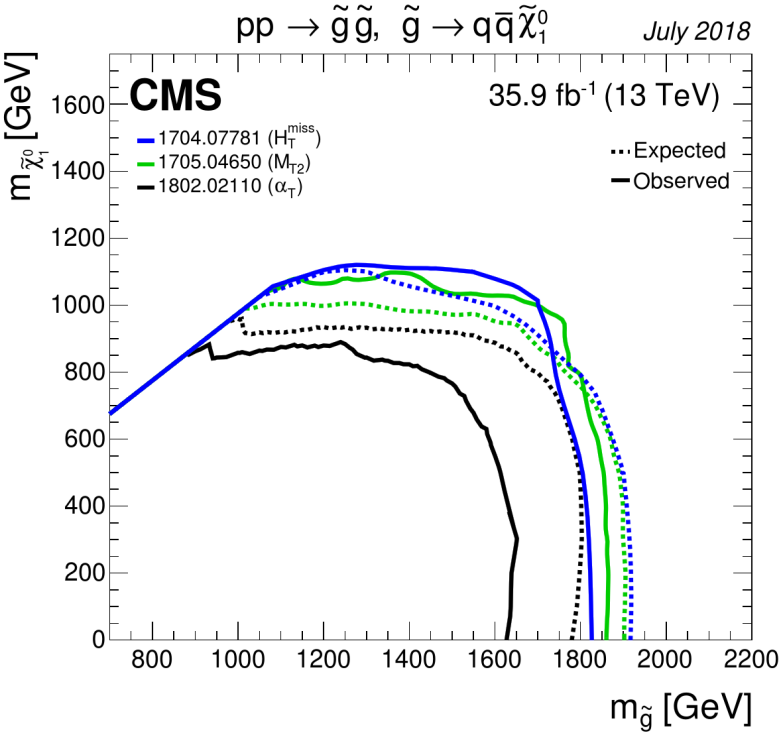
pp → g̃ g̃, g̃ → q q̄ χ̃⁰₁
July 2018
CMS
35.9 fb⁻¹ (13 TeV)
1704.07781 (H_T^miss)
1705.04650 (M_T2)
1802.02110 (α_T)
Expected
Observed
m_χ̃⁰₁ [GeV]
m_g̃ [GeV]

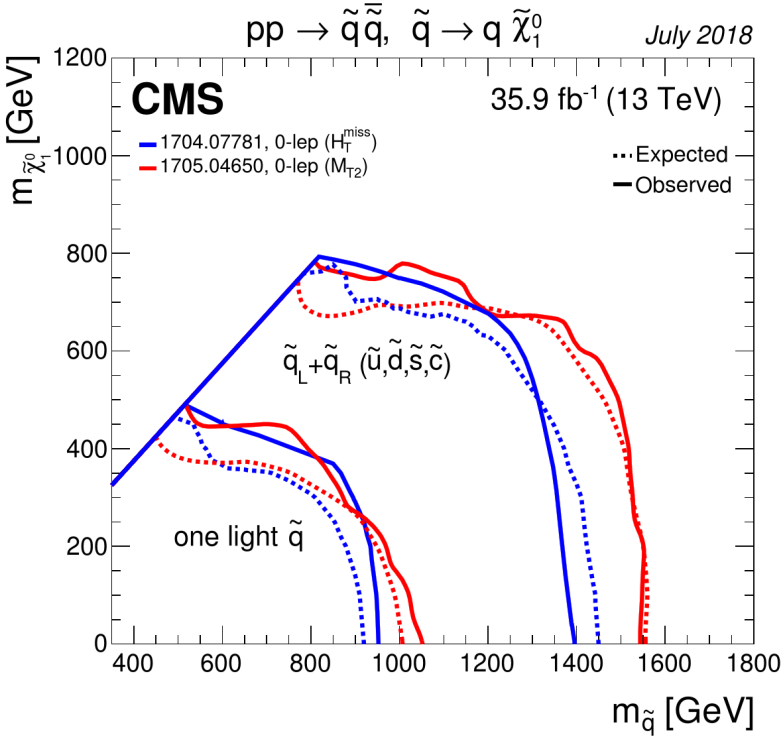
pp → q̃ q̃̄, q̃ → q χ̃⁰₁
July 2018
CMS
35.9 fb⁻¹ (13 TeV)
1704.07781, 0-lep (H_T^miss)
1705.04650, 0-lep (M_T2)
Expected
Observed
q̃_L+q̃_R (ũ,d̃,s̃,c̃)
one light q̃
m_χ̃⁰₁ [GeV]
m_q̃ [GeV]

Relevant Constraints

- Higgs mass, $122 < m_h(GeV) < 128$.
- Lower limits on sparticle masses from colliders
- Flavour physics constraints
- Dark matter constraints (underabundance allowed)

Constraints from Higgs mass

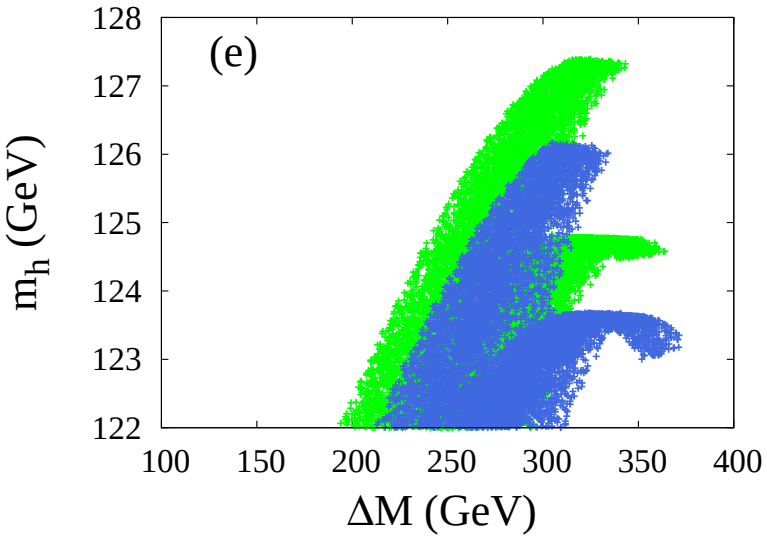

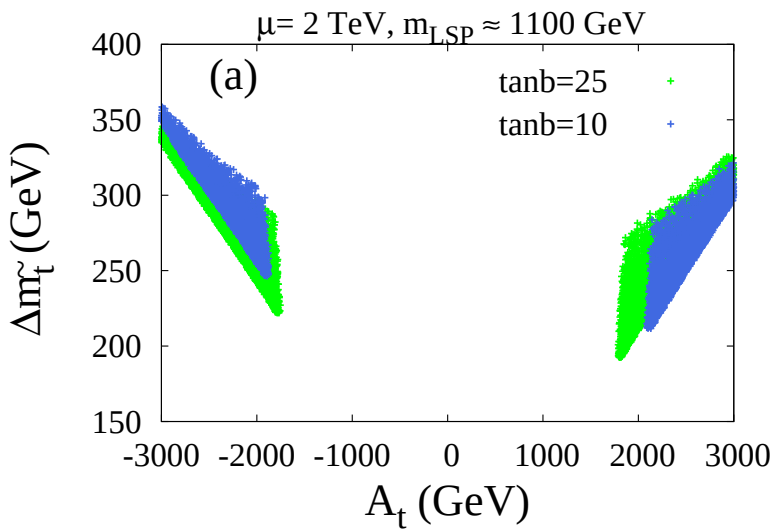

Constraints from DM Direct Detection

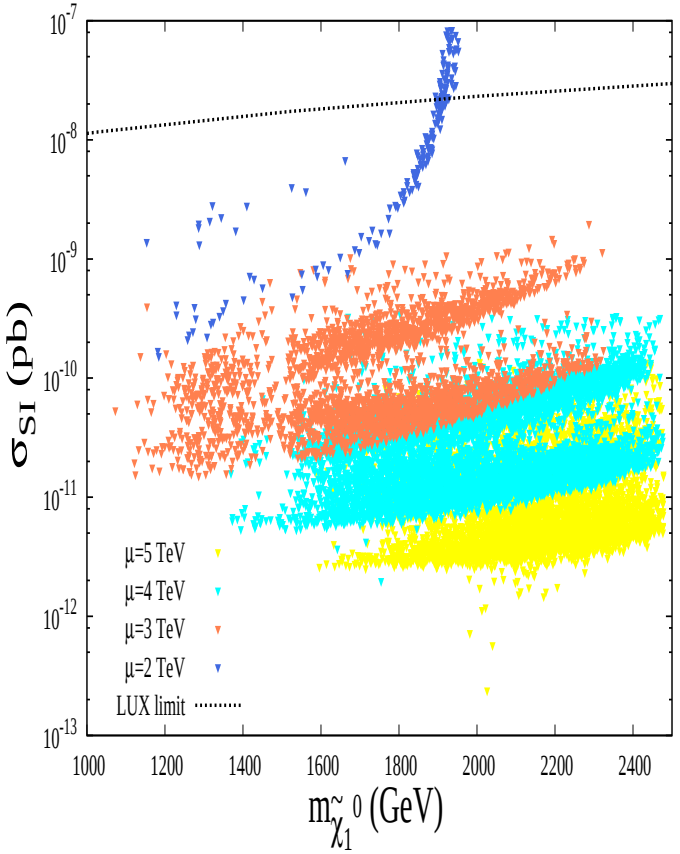

$\widetilde{\chi}_1^0$ LSP and cold dark matter candidate, satisfies observed thermal relic density.

Low μ values, ($\sim$ 2 TeV) strongly constrained from direct detection cross-section data from LUX due to large bino-higgsino mixing.

Signals & Results

We consider the following signals at $\sqrt{s} = 13$ TeV for our study :

- Monojet + $\not{E}_T$ (CMS criteria)
- Multijets (≥ 2 j) + $\not{E}_T$

Simulation Details

SUSY signal: $\widetilde{q}\widetilde{g}$, $\widetilde{q}\widetilde{q}$, $\widetilde{q}\widetilde{q}^*$, $\widetilde{g}\widetilde{g}$ + $\leq$ 2 partons.

- Model Files: `SARAH`
- Spectrum Generator: SPheno
- Madgraph5 $\rightarrow$ Pythia $\rightarrow$ Delphes-v3 for event generation, showering and detector simulation.
- MLM matching with showerKT performed duly with QCUT = 120 GeV (SUSY), 30−50 GeV (SM).

Benchmarks

Parameters	BP1	BP2
A_t	-1535.1	2300.0
μ	3000.0	3000.0
$\tan\beta$	23.9	20.0
$m_{\widetilde{g}}$	1497.4	1534.7
$m_{\widetilde{q}_L}$	1452.3	1524.5
$m_{\widetilde{q}_R}$	1451.3	1520.8
$m_{\widetilde{t}_1}$	1330.6	1507.6
$m_{\widetilde{t}_2}$	1509.0	1686.6
$m_{\widetilde{b}_1}$	1407.4	1521.9
$m_{\widetilde{b}_2}$	1494.5	1619.5
$m_{\widetilde{\chi}_1^0}$	1323.9	1496.3
$m_{\widetilde{\chi}_2^0}$	1342.9	1559.0
$m_{\widetilde{\chi}_1^\pm}$	1342.9	1559.1
m_h	122.5	122.4
Ωh^2	0.113	0.105
$\sigma_{SI} \times 10^{11}$ (pb)	4.65	0.13
ΔM_i (GeV)	173.5	38.4

$\Delta M_i = m_S - m_{\widetilde{\chi}_1^0}$, where $S \in [\widetilde{q}, \widetilde{g}]$

Differential distributions of kinematic variables

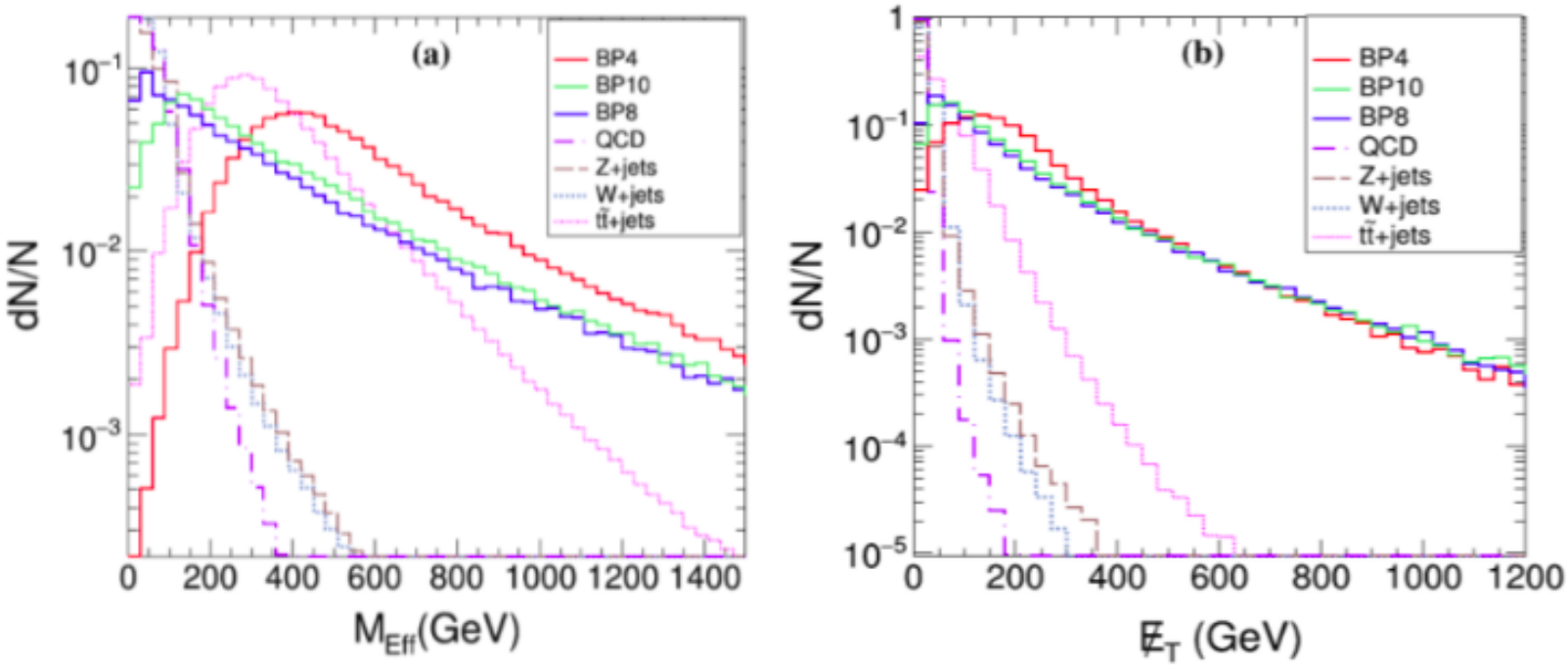

Effective Mass, $M_{Eff} = \Sigma_i p_{T_i} + \not{E}_T$, i runs over all visible objects

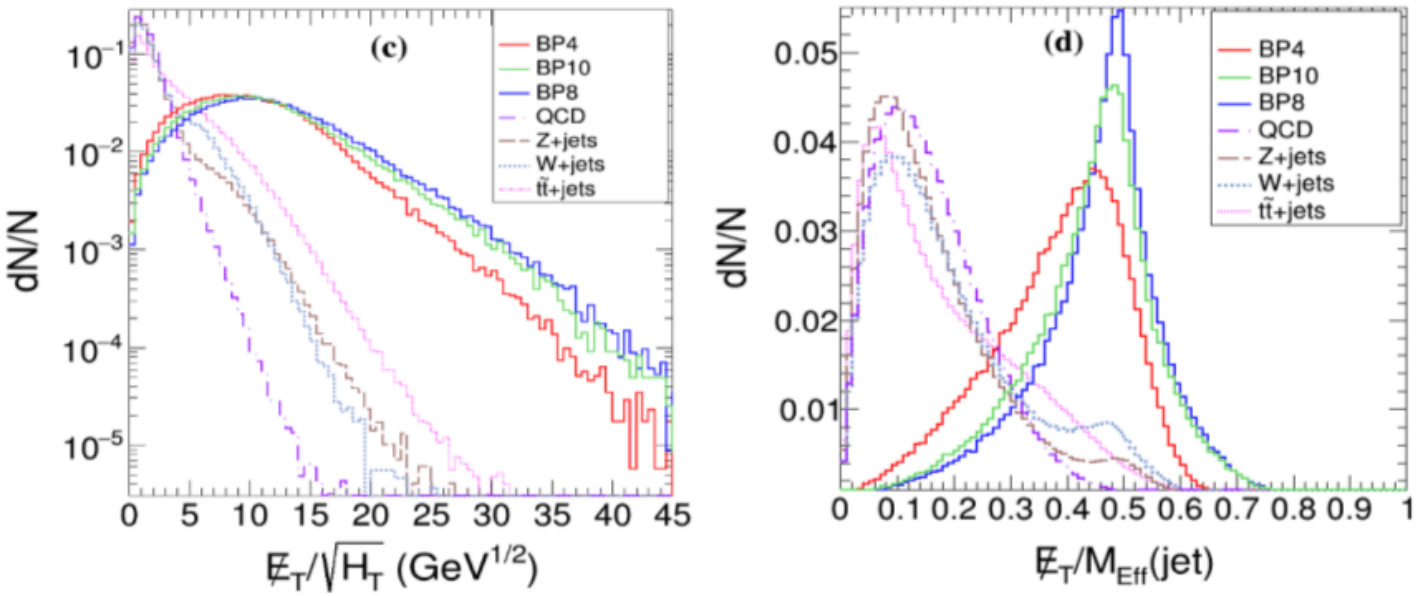

Variables: $\not{E}_T/\sqrt{H_T}$, $\not{E}_T/M_{Eff}$ used by ATLAS for multijet searches.

Employing optimal cuts on various kinematical observables (i.e, $\not{E}_T$, M_{Eff},..) for multijet and monojet searches at LHC:

Signal		Cross-section after cuts (fb)				
Benchmark Points	Production cross-section(fb)	Preselection	M_{Eff} > 800 GeV	$\not{E}_T$ > 160 GeV	$\not{E}_T/\sqrt{H_T}$ $> 15\text{GeV}^{1/2}$	$\not{E}_T/M_{Eff}$ > 0.35
BP1	126.93	59.72	20.74	19.84	9.99	9.93
BP2	95.58	12.45	6.34	6.24	4.72	4.68
SM Background	2.0E+08	253042	2833	8.85	1.36	1.35

Multijets + $\not{E}_T$ cross-section for signal and background (at NLO).

(Preselection: $p_T(j_1) > 130$ GeV, $p_T(j_2) > 80$ GeV, $\Delta\phi(j_{1/2}, \not{E}_T) > 0.4$)

Signal		Cross-section after cuts (fb)		
Benchmark Points	Production cross-section(fb)	Preselection	$\not{E}_T$ >160 GeV	M_{Eff} >800 GeV
BP1	126.93	12.06	8.22	0.88
BP2	95.58	7.48	6.20	1.63
SM background	2×10^8	46254	2602	0.938

Monojet + $\not{E}_T$ cross-section for signal and background (at NLO).

(Preselection: $p_T(j_1) > 130$ GeV, $\Delta\phi(j_1, \not{E}_T) > 1, p_T(j_2) < 80$ GeV, $\Delta\phi(j_2, \not{E}_T) > 1$)

	Luminosity (in fb^{-1}) for 3σ excess	
Signal	BP1	BP2
Multijets (≥ 2 j) + $\not{E}_T$	123	558
Monojet + $\not{E}_T$	10926	3204

- Multijet + met searches still more efficient to look for compressed scenarios than traditional monojet + met channels.
- However both are viable modes of discovery for compressed spectra at the Run 2 of LHC.

Case II: Compression in MSSM + $\widetilde{G}$ LSP

- We focus on a compressed MSSM spectra with a bino-like $\widetilde{\chi}_1^0$ NLSP extended with a keV gravitino LSP.

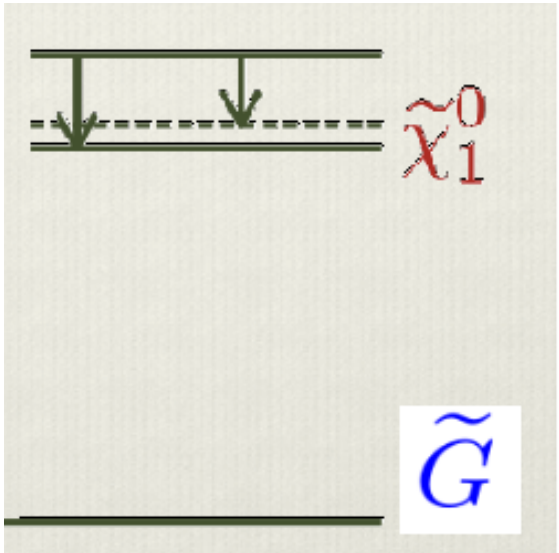

- Presence of light $\widetilde{G}$ relaxes DM constraints on $\widetilde{\chi}_1^0$.

Branching ratios of $\widetilde{X}$

- $\Gamma(\widetilde{X} \to X\widetilde{G}) \propto m_{\widetilde{X}}^{5} m_{\widetilde{G}}^{-2}$

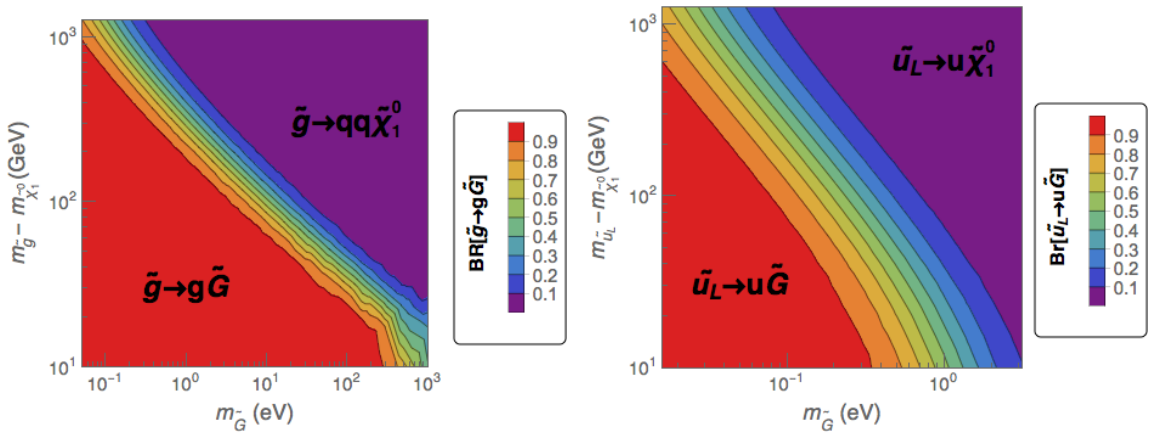

- Small compression ($\Delta M \sim 50$ GeV) and $m_{\widetilde{G}} \sim 1$ keV : $\mathrm{BR}(\widetilde{g} \to q\bar{q}\widetilde{\chi}_1^0) > \mathrm{BR}(\widetilde{g} \to g\widetilde{G})$.
- Large compression ($\Delta M \sim 10$ GeV) and $m_{\widetilde{G}} \sim 1$ keV: $\mathrm{BR}(\widetilde{g} \to q\bar{q}\widetilde{\chi}_1^0) < \mathrm{BR}(\widetilde{g} \to g\widetilde{G})$.
- For sub-keV $\widetilde{G}$: $\mathrm{BR}(\widetilde{g} \to g\widetilde{G})$ dominant.

- The bino-like $\widetilde{\chi}_1^0$ NLSP decays dominantly to γ and $\widetilde{G}$ and a small fraction to $Z + \widetilde{G}$. This leads to extremely hard photons and large $\not{E}_T$.

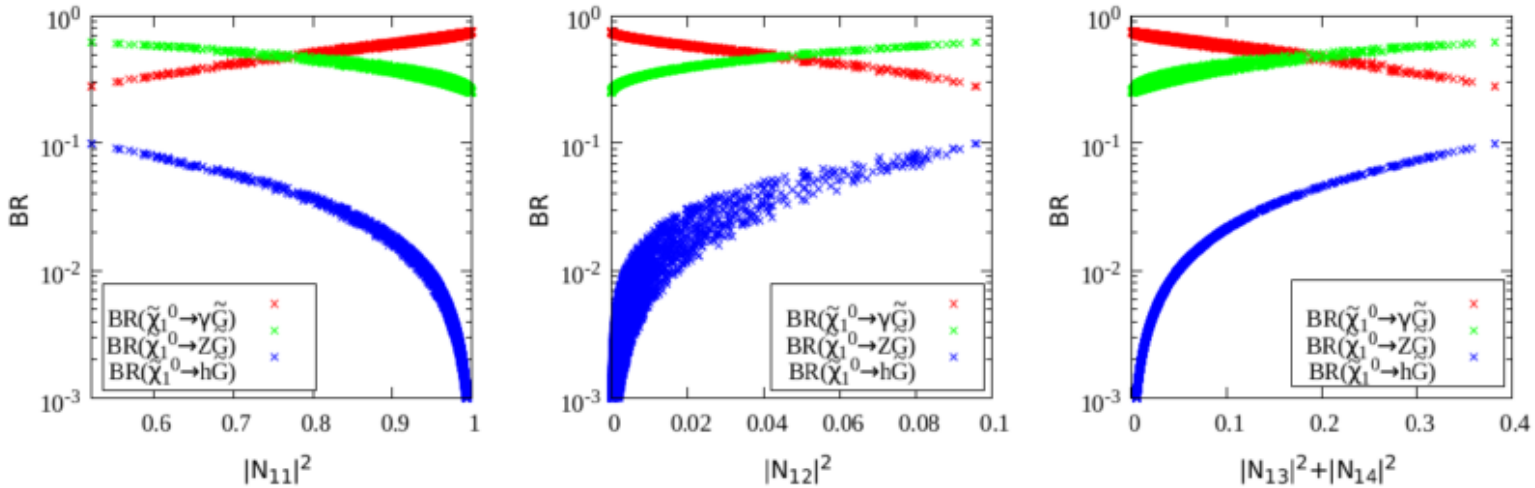

- These hard photon associated signals can be very effective to probe a heavy compressed SUSY spectra with a light gravitino as there would be rarely any Standard Model events with such hard photons.

Signals and Results

We consider the following signal:

- $\geq 1\gamma + > 2j + \not{E}_T$

Experimental collaborations (ATLAS−CONF−2016−66) consider signal events coming from gluino pair production only, assuming rest of the sparticles decoupled, ruling out $m_{\tilde{g}} \leq 1.95$ TeV for $m_{\tilde{\chi}_1^0} \sim 1.8$ TeV.

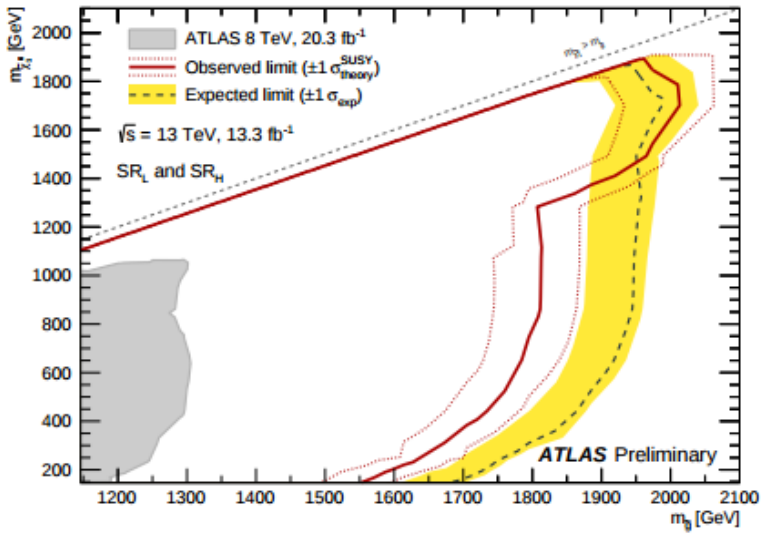

- However for a compressed spectra, presence of closely spaced sparticles lead to added contributions to the same final state.
- Thus, the limits on sparticles are stronger for a compressed spectra.

Using the ATLAS analysis for $\geq 1\gamma + > 2$ jets $+ \not{E}_T$ and SM background estimates at 13.3 fb^{-1}, mass bounds significantly increase for a compressed spectra, i.e, $m_{\widetilde{g}/\widetilde{q}} \geq 2.5$ TeV.

Hard photons are a characteristic feature of both compressed and uncompressed spectra.

Benchmarks

	Compressed spectra		Uncompressed spectra
Parameters	**C4**	**C5**	**U2**
A_t	-3750	-3197	2895
μ	4000	3500	3000
$\tan\beta$	6	25	15
M_A	1800	2500	2500
$m_{\widetilde{g}}$	2783	2562	2102
$m_{\widetilde{q}_L}$	2753	2571	4721
$m_{\widetilde{q}_R}$	2751	2574	4742
$m_{\widetilde{t}_1}$	2625	2532	4678
$m_{\widetilde{t}_2}$	2863	2718	4765
$m_{\widetilde{b}_1}$	2778	2594	4558
$m_{\widetilde{b}_2}$	2846	2677	4744
$m_{\widetilde{\chi}_1^0}$	2585	2526	1191
$m_{\widetilde{\chi}_2^0}$	2724	2619	2383
$m_{\widetilde{\chi}_1^\pm}$	2724	2619	2382
m_h	124	125	125
ΔM_i	198	48	911

Using the existing ATLAS analysis cuts (using hard cuts on photon p_T and $\not{E}_T$) and SM background estimates at 13.3 fb^{-1} for the same final state:

Signal		Cross-section (in fb) after cuts					
Benchmark Points	Production cross-section(fb)	$p_T(\gamma_1)$ > 400	$N_j > 2$ $N_l = 0$	$\Delta\phi(j_{1/2}, \not{E}_T)$ > 0.4	$\Delta\phi(\gamma_1, \not{E}_T)$ > 0.4	$\not{E}_T$ > 400	M_{Eff} > 2000
C4	0.21	0.15	0.12	0.08	0.08	0.08	0.07
C5	0.49	0.34	0.15	0.13	0.13	0.12	0.11
U2	0.20	0.13	0.12	0.10	0.09	0.08	0.08

we compute the required luminosity for some benchmarks:

Signal	Luminosity $\mathcal{L}$ (in fb^{-1}) for	
	$\mathcal{S} = 3\sigma$	$\mathcal{S} = 5\sigma$
C4	176	489
C5	79	219
U2	139	385

Using $p_T(\gamma)$, $p_T(j)$ and N_j, a set of new kinematic variables identified which act as a discriminant for a compressed and uncompressed spectra with similar event rates:

$$r_1' = N_j r_1,\ r_2' = N_j r_2,\ \text{where } r_1 = \frac{p_T(j_1)}{p_T(\gamma_1)}, r_2 = \frac{p_T(j_2)}{p_T(\gamma_1)}$$

For **C4**, **C5**: $r_1' \sim 0.2 - 0.5$, $r_2' \sim 0.1 - 0.3$ while for **U2**: $r_1' \sim 4$, $r_2' \sim 2.5$.

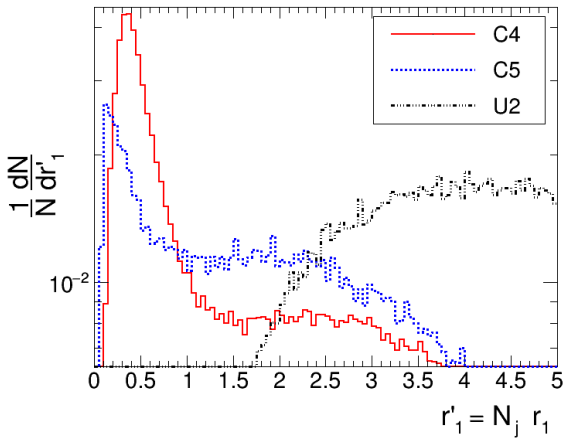

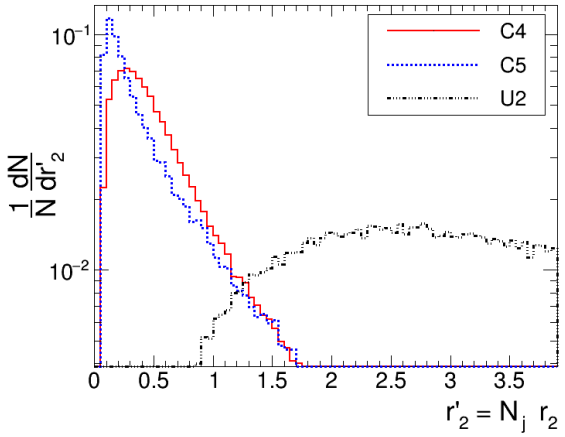

Case III: Low lying higgsino sector with $\widetilde{\nu}_R$ LSP

- We focus on the low μ sector $\rightarrow$ naturally compressed $\widetilde{\chi}_1^0, \widetilde{\chi}_2^0, \widetilde{\chi}_1^{\pm}$.
- Rest of the spectrum decoupled.
- Presence of $\widetilde{\nu}_R$ LSP opens up new leptonic channels for the higgsinos $\rightarrow$ lepton modes for discovery.

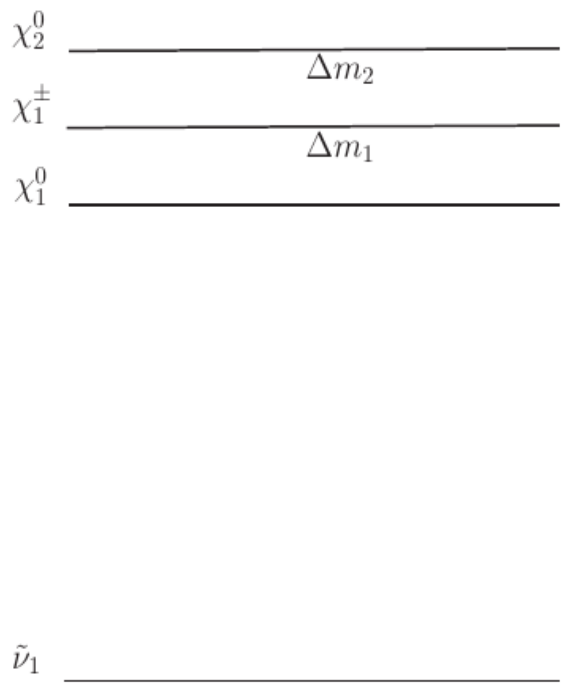

Sneutrino Sector

- In the CP basis, the sneutrino mass matrix is:

$$\mathcal{M}^{j\ 2} = \begin{pmatrix} m^2_{LL} & m^{j2}_{LR} \\ m^{j\ 2}_{LR} & m^{j\ 2}_{RR} \end{pmatrix},$$

where,

$$\begin{aligned} m^2_{LL} &= m^2_L + \frac{1}{2} m^2_Z \cos 2\beta + m^2_D, \\ m^{j\ 2}_{LR} &= (T_\nu \pm y_\nu M_R) v \sin\beta - \mu m_D \cot\beta, \\ m^{j\ 2}_{RR} &= m^2_R + m^2_D + M^2_R \pm B_M, \end{aligned} \tag{1}$$

j = even, odd states and $m_D = y_\nu v_u$, the Dirac mass obtained by SM neutrinos after electroweak symmetry breaking, i.e, $< H^0_u >= v_u$.

- Diagonalizing the mass matrix, the mass eigenvalues are given by:

$$m^{j\,2}_{1,2} = \frac{1}{2}\left(m^2_{LL} + m^{j\,2}_{RR} \pm \sqrt{(m^2_{LL} - m^{j\,2}_{RR})^2 + 4m^{j\,4}_{LR}}\right). \quad (2)$$

- Presence of non-zero B_M generates a mass split between the sneutrino mass eigenstates.
- Left-right mixing angle θ in the sneutrino sector,

$$\sin 2\theta^j = \frac{(T_\nu \pm y_\nu M_R)v \sin\beta - \mu m_D \cot\beta}{m^{j2}_2 - m^{j2}_1}, \quad (3)$$

- Choice of $T_\nu \sim \mathcal{O}(1)\mathrm{GeV}$ leads to increased mixing in the sneutrino sector.
- Radiative contribution to neutrino mass arise in presence of non-zero B_M, T_ν from sneutrino-gaugino loops.

Constraints on $B_M - T_\nu$ parameter space.

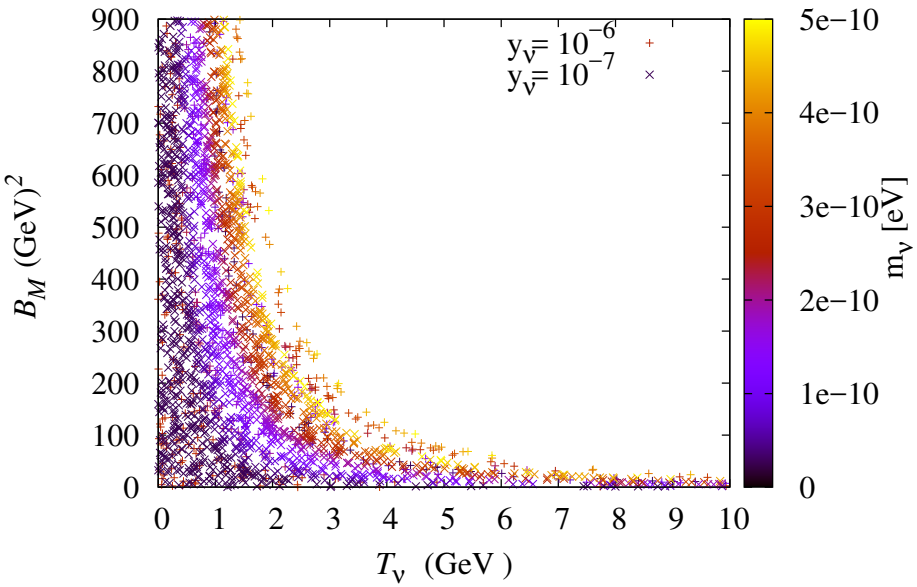

Figure: Allowed regions of B_M and T_ν plane for $M_1 = 1.5$ TeV, $M_2 = 1.8$ TeV and gaugino fraction $\sim \mathcal{O}(10^{-2})$. The colored palette denotes the mass of the heaviest neutrino. We consider $y_\nu \in \{10^{-6}, 10^{-7}\}$, $\mu = 300$ GeV, $M_3 = 2$ TeV, $M_{Q_3} = 1.5$ TeV, $T_t = 2.9$ TeV, $M_{L_{1/2}} = 600$ GeV, $m_{\tilde{\nu}}^{soft} = 100$ GeV and $M_A = 2.5$ TeV.

Large B_M and large T_ν stringently constrained from neutrino mass.

Spectra of interest

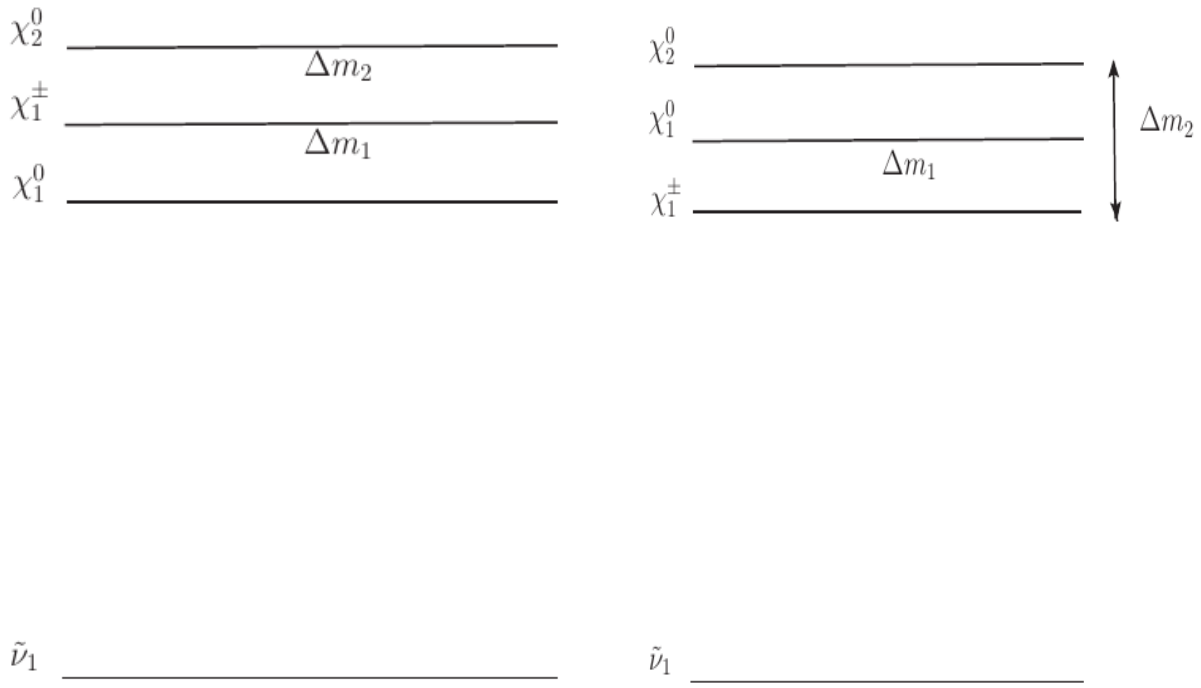

Figure: Schematic description of the mass spectrum with $|M_1|, M_2 \gg |\mu|$, and $m_{\tilde{\nu}_1} < |\mu|$. Here $|m_{\tilde{\chi}_2^0}| - m_{\tilde{\chi}_1^\pm} = \Delta m_2$, $m_{\tilde{\chi}_1^\pm} - |m_{\tilde{\chi}_1^0}| = \Delta m_1$. Here, $M_1, M_2 \sim \mathcal{O}(1)$TeV.

Effect of M_1, M_2 on the higgsino sector

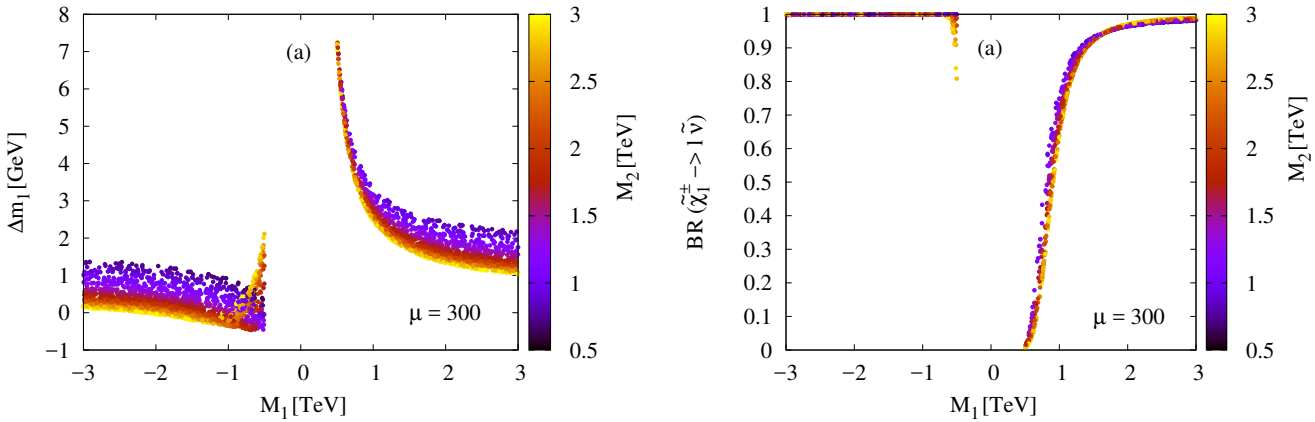

Figure: The left (right) panel shows the variation of the mass difference $\Delta m_1 = m_{\widetilde{\chi}_1^\pm} - m_{\widetilde{\chi}_1^0}$ between $\tilde{\chi}_1^\pm$ and $\tilde{\chi}_1^0$ and BR($\widetilde{\chi}_1^\pm \to l\widetilde{\nu}$) for tan $\beta = 5$ with respect to M_1, with M_2 on the palette. The other relevant parameters are $\mu = 300\text{GeV}$, $T_t = 2.9$ TeV, $M_{Q_3} = 1.3$ TeV, $M_{U_3} = 2$ TeV and $M_3 = 2$ TeV.

Collider Signatures

SUSY signals: $\widetilde{\chi}_1^0\widetilde{\chi}_2^0$, $\widetilde{\chi}_1^\pm\widetilde{\chi}_1^0$, $\widetilde{\chi}_1^\pm\widetilde{\chi}_1^\pm$, $\widetilde{\chi}_1^+\widetilde{\chi}_1^-$

- $1\ l + \leq 1\ j + \not{E}_T$ (Mono-lepton)
- $2\ l\ (\ l^+l^-) + 0\ j + \not{E}_T$ (Opposite-sign dilepton)
- $2\ l\ (\ l^\pm l^\pm) + 0\ j + \not{E}_T$ (Same sign dilepton)

- Utilising low jet multiplicity(n_{jet}), transverse mass M_T, missing transverse energy ($\not{E}_T$), M_{T_2} to remove dominant SM backgrounds: W+j, $t\bar{t}$,Drell Yan, WZ.
- $t\bar{t}$ backgrounds reduced using b-veto, $n_{jet} \leq 1$, $M_T(l, \not{E}_T)$ and $\not{E}_T > 100$ GeV for mono-lepton. For dilepton, $n_{jet} = 0$ and M_{T_2} cut further reduces $t\bar{t}$ significantly.

Benchmarks

Parameters	BP1	BP2	BP3	BP4	BP5	BP6	BP7	BP8	BP9	BP10
M_1	1470.0	850.0	1107.0	1334.5	1476.3	1890.3	1200.0	1510.0	1105.0	1730.0
M_2	1400.5	880.0	1200.0	1328.6	1402.6	1971.3	1250.0	1550.0	1150.0	1770.0
M_3	1312.0	780.0	1015.0	1405.5	1387.7	1737.1	1180.0	1420.0	1080.0	1600.0
A_t	2200.8	-1650.0	1897.0	-1535.1	1840.8	2800.2	2050.0	2300.0	2000.0	2720.0
μ	2000.0	3000.0	2000.0	3000.0	3000.0	2000.0	2500.0	3000.0	3000.0	2000.0
$\tan\beta$	20.0	20.0	25.0	23.9	24.2	16.87	18.0	20.0	20.0	35.0
$m_{\widetilde{g}}$	1429.5	861.6	1112.8	1497.4	1500.4	1882.0	1276.7	1534.7	1165.6	1737.8
$m_{\widetilde{q}_L}$	1476.2	893.7	1159.4	1452.3	1532.8	1912.6	1271.6	1524.5	1129.0	1790.0
$m_{\widetilde{q}_R}$	1474.3	887.4	1158.1	1451.3	1531.9	1910.6	1270.2	1520.8	1130.7	1794.5
$m_{\widetilde{t}_1}$	1412.3	871.7	1097.9	1330.6	1426.1	1865.0	1192.4	1507.6	1100.4	1711.3
$m_{\widetilde{t}_2}$	1595.9	1136.8	1300.4	1509.0	1581.3	2045.6	1390.5	1686.6	1308.3	1903.2
$m_{\widetilde{b}_1}$	1459.7	861.6	1137.1	1407.4	1493.5	1966.7	1249.6	1521.9	1130.4	1761.3
$m_{\widetilde{b}_2}$	1525.3	1044.1	1224.7	1494.5	1570.3	2011.6	1323.6	1619.5	1229.4	1838.4
$m_{\widetilde{\ell}_L}$	1432.7	880.9	1121.2	1400.7	1482.7	1916.4	1221.8	1543.9	1132.8	1745.8
$m_{\widetilde{\ell}_R}$	1426.2	871.0	1114.7	1400.7	1482.7	1907.6	1215.4	1536.0	1121.7	1736.9
$m_{\widetilde{\tau}_1}$	1430.3	890.3	1113.5	1353.2	1438.0	1893.7	1220.0	1529.1	1105.6	1725.4
$m_{\widetilde{\tau}_2}$	1483.8	1003.3	1209.5	1446.6	1526.0	1928.4	1289.1	1602.2	1198.2	1803.8
$m_{\widetilde{\nu}_L}$	1429.8	876.5	1117.6	1398.6	1480.6	1914.4	1218.3	1540.5	1128.9	1743.1
$m_{\widetilde{\chi}_1^0}$	1406.4	842.4	1096.3	1323.9	1417.6	1862.0	1189.0	1496.3	1095.4	1709.3
$m_{\widetilde{\chi}_2^0}$	1453.9	889.1	1200.8	1342.9	1463.6	1934.7	1256.9	1559.0	1158.0	1764.9
$m_{\widetilde{\chi}_1^\pm}$	1406.7	889.3	1201.0	1342.9	1417.6	1929.1	1257.1	1559.1	1158.2	1764.3
m_h	122.6	122.0	122.2	122.5	122.8	123.9	122.0	122.4	122.1	124.6
Ωh^2	0.092	0.032	0.036	0.113	0.099	0.113	0.062	0.105	0.073	0.110
$\sigma_{SI} \times 10^{11}$ (pb)	115.78	50.11	35.95	4.65	9.08	744.98	7.64	0.13	9.56	280.97
ΔM (GeV)	189.5	294.4	204.1	185.1	163.7	183.6	201.5	190.3	212.9	193.9
ΔM_i (GeV)	69.8	51.3	63.1	173.5	115.2	50.6	87.7	38.4	70.2	85.2

Benchmarks

Parameters	**BP2−a**	**BP4**
μ	-500	400
$\tan\beta$	5	6.1
M_1	1500	-1150
M_2	1800	2500
M_A	803.2	2500
$Y_\nu(\times 10^{-7})$	10	1
$m_{\widetilde{\chi}_1^\pm}$	510.9	407.2
$m_{\widetilde{\chi}_1^0}$	508.4	407.3
$m_{\widetilde{\chi}_2^0}$	512.2	407.5
$m_{\widetilde{\nu}_R}$	412.2	331.7
m_h	124.1	124.7
Δm_1	2.5	-0.1
Δm_2	3.8	0.2
ΔM	96.2	75.5
Ωh^2	0.11	
σ_{SI} (pb)	1.4×10^{-10}	
$\sin\theta^j(\times 10^{-2})$	10.9	0.004
$BR(\widetilde{\chi}_1^\pm \to l\ \widetilde{\nu})$	1.00	1.0
$BR(\widetilde{\chi}_2^0 \to W^{\mp *}\ \widetilde{\chi}_1^\pm \to l\widetilde{\nu}\ W^{*\mp})$	0.0	0.10

Collider study

BP2-a	$\mathcal{L} = 3\sigma\ (fb^{-1})$	$\mathcal{L} = 5\sigma\ (fb^{-1})$
$1l + \leq 1j + \not{E}_T$	1384	3485
$l^+l^- + \leq 1j + \not{E}_T$	51	142
$l^\pm l^\pm + \leq 1j + \not{E}_T$	-	-
BP4	$\mathcal{L} = 3\sigma\ (fb^{-1})$	$\mathcal{L} = 5\sigma\ (fb^{-1})$
$1l + \leq 1j + \not{E}_T$	448	1245
$l^+l^- + \leq 1j + \not{E}_T$	160	444
$l^\pm l^\pm + \leq 1j + \not{E}_T$	1085	3845

Results

- Monolepton channel with low hadronic activity is the best channel for large $\Delta M = (m_{NLSP} - m_{LSP})(> 50)$ GeV and moderate $BR(\widetilde{\chi}_1^{\pm} \to l\widetilde{\nu}) \sim 0.1 - 0.3$.
- For large $BR(\widetilde{\chi}_1^{\pm} \to l\widetilde{\nu})(\sim 1.0) \implies$ opposite sign dilepton channels most favoured.
- Same sign dileptons $\implies$ strong confirmatory channels for a sneutrino LSP over $\widetilde{\chi}_1^0$ LSP.

Conclusions

- Compressed spectra in MSSM with $\widetilde{\chi}_1^0$ LSP stringently constrained from higgs mass.
- Such scenarios gives rise to multiple jets and $\not{E}_T$ which fare better over traditional monojet and $\not{E}_T$ signal.
- Extensions of MSSM with $\widetilde{\chi}_1^0$ as NLSP and light $\widetilde{G}$ or $\widetilde{\nu}_R$ as LSP open up alternate channels to probe compressed spectra.
- Limits on compressed spectra more stringent in the presence of hard photons signals.

- A low-lying higgsino sector is challenging to study in MSSM owing to its natural compression and low production cross-sections. Presence of non-standard LSP help probe this sector.
- However, viability of low μ parameter, hence a light higgsino sector, depends crucially on the choice of the gaugino parameters, M_1, M_2.
- In the presence of $\widetilde{\nu}_R$ LSP, leptonic channels with upto two leptons with low hadronic activity and missing energy observable at LHC.

Thank You

Backup

Benchmarks

Parameters	BP1	BP2	BP3	BP4	BP5	BP6	BP7	
A_t	2200.8	-1650.0	1897.0	-1535.1	1840.8	2800.2	2050.0	2
μ	2000.0	3000.0	2000.0	3000.0	3000.0	2000.0	2500.0	3
$\tan\beta$	20.0	20.0	25.0	23.9	24.2	16.87	18.0	
$m_{\widetilde{g}}$	1430.0	861.6	1111.6	1497.4	1500.4	1882.0	1275.9	1
$m_{\widetilde{q}_L}$	1475.1	893.7	1159.0	1451.2	1532.8	1912.6	1271.4	1
$m_{\widetilde{q}_R}$	1473.6	887.4	1158.1	1450.9	1531.9	1909.9	1269.9	1
$m_{\widetilde{t}_1}$	1412.3	871.7	1097.9	1330.6	1426.1	1865.0	1192.4	1
$m_{\widetilde{t}_2}$	1595.9	1136.8	1300.4	1509.0	1581.3	2045.6	1390.5	1
$m_{\widetilde{b}_1}$	1459.7	861.6	1125.1	1407.4	1493.5	1966.7	1241.9	1
$m_{\widetilde{b}_2}$	1525.3	1044.1	1222.3	1494.5	1570.3	2011.6	1321.7	1
$m_{\widetilde{\chi}_1^0}$	1406.7	842.4	1096.1	1323.9	1417.6	1861.9	1188.9	1
$m_{\widetilde{\chi}_2^0}$	1453.9	889.1	1200.6	1342.9	1463.6	1934.7	1256.9	1
$m_{\widetilde{\chi}_1^\pm}$	1407.0	889.3	1200.8	1342.9	1417.6	1929.1	1257.1	1
m_h	122.6	122.0	122.2	122.5	122.8	123.9	122.0	1
Ωh^2	0.092	0.032	0.036	0.113	0.099	0.113	0.062	(
$\sigma_{SI} \times 10^{11}$ (pb)	115.78	50.11	35.95	4.65	9.08	744.98	7.64	
ΔM_i (GeV)	68.4	51.3	41.6	173.5	115.2	50.7	87.0	

Electroweakino sector

- Naturalness $\Longrightarrow$ low μ $\Longrightarrow$ low-lying compressed higgsinos
- In the limit $M_1, M_2 \gg |\mu|$,

$$m_{\widetilde{\chi}_1^{\pm}} = |\mu|(1 - \frac{M_W^2 \sin 2\beta}{\mu M_2}) + \mathcal{O}({M_2}^{-2}) + \text{rad. corr.}$$

$$m_{\widetilde{\chi}^0_{a,s}} = \pm\mu - \frac{M_Z^2}{2}(1 \pm \sin 2\beta)(\frac{\sin\theta_W^2}{M_1} + \frac{\cos\theta_W^2}{M_2}) + \text{rad. corr.}$$

where the subscripts s(a) denote symmetric (anti-symmetric) higgsino states respectively (M.Drees et.al, hep-ph/9701219).

Effect of M_1, M_2 on the higgsino sector

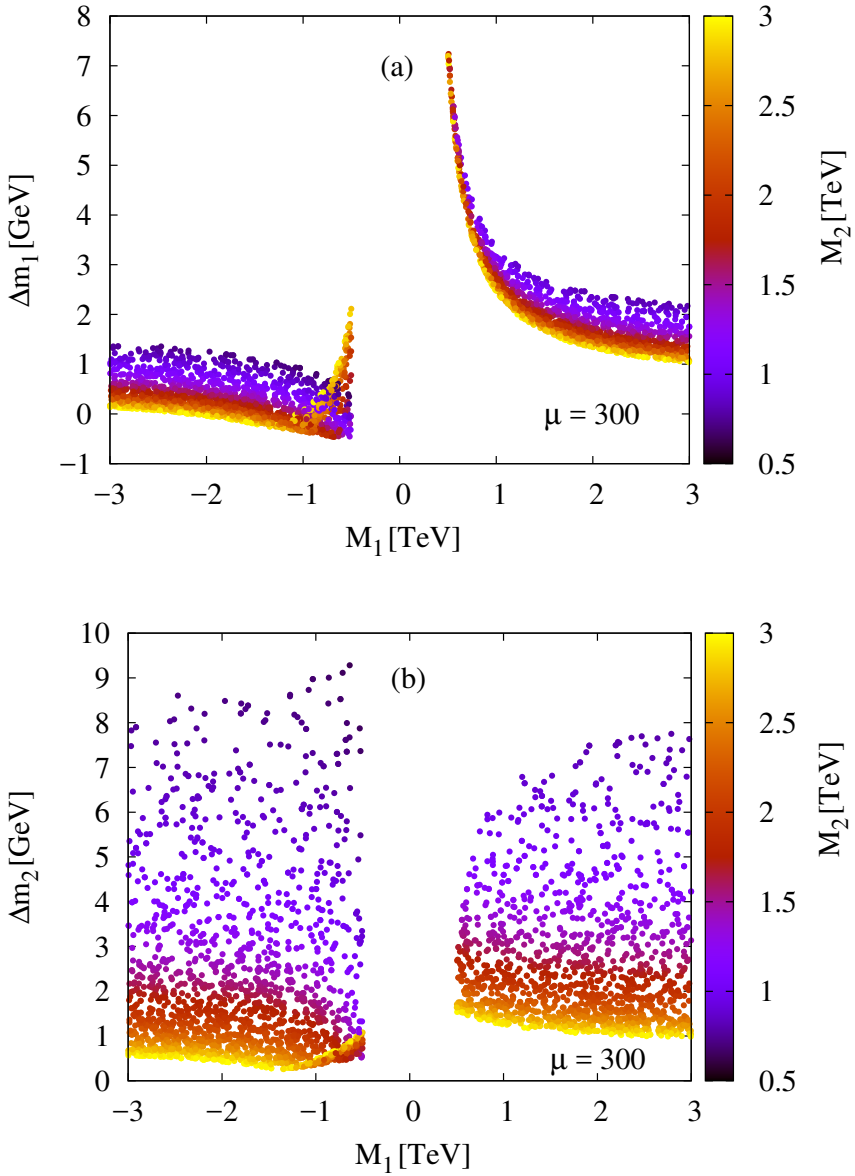

Decays of higgsinos

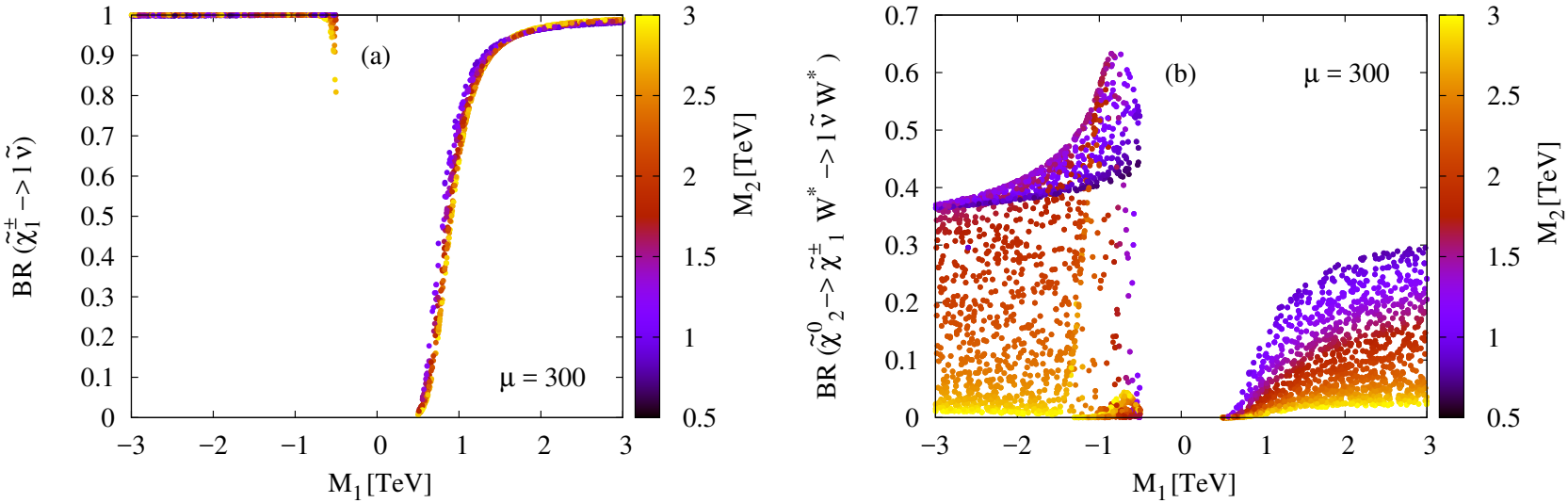

Figure: Variation of the leptonic branching ratios of $\widetilde{\chi}_1^{\pm} \to l\widetilde{\nu}$ and $\widetilde{\chi}_2^0 \to l\widetilde{\nu}W^*$ against the bino soft mass parameter, M_1 for the Higgsino mass parameter, $\mu = 300$ GeV. The wino soft mass parameter M_2 is shown in the palette. $T_\nu > 10^{-2}$ GeV for prompt decay of $\widetilde{\chi}_1^{\pm}$.

Presence of sneutrino LSP opens up new leptonic channels for the compressed higgsinos.

Right sneutrino as Dark Matter

For $y_\nu \sim 10^{-6} - 10^{-7}$, co-annihilation of DM with the higgsinos give correct, Ωh^2_{DM}. Further, m_{DM} at higgs or heavy higgs resonance also lead to correct relic density.

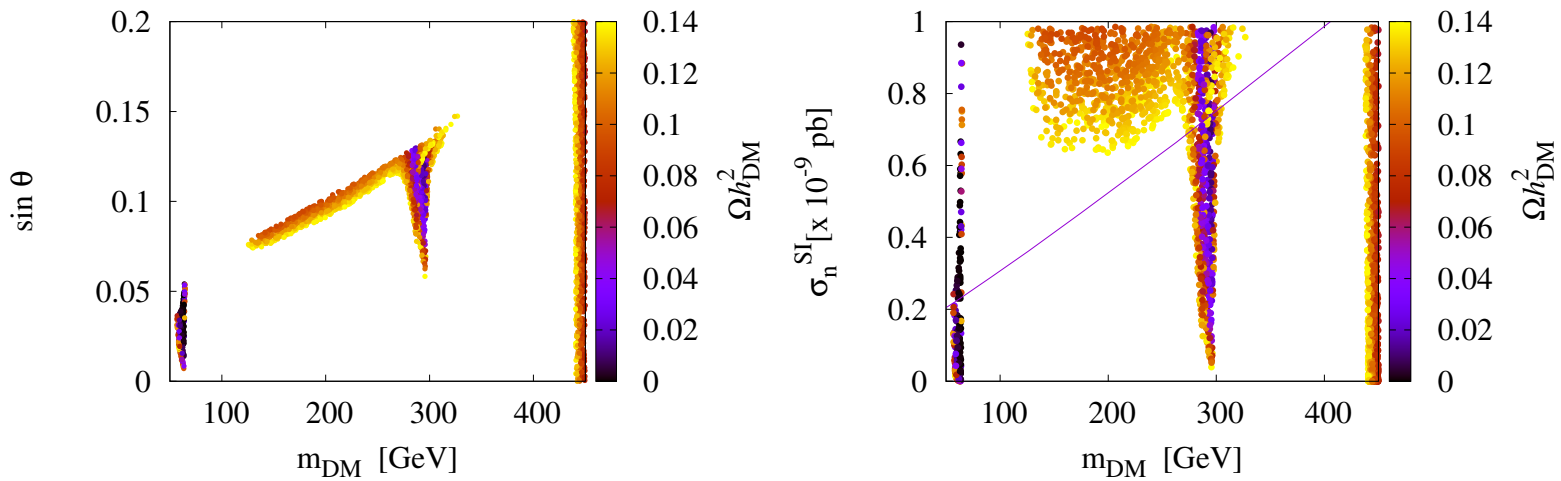

Figure: Dependence of the relic abundance of $\tilde{\nu}_1$ on its mass vs. left-sneutrino fraction and direct detection constraint from `XENON-1T` for $|\mu| = 450$ GeV, $M_A = 600$ GeV and rest as before.

Motivations

- Higgs mass receives large contributions at one-loop level from SM particles and other particles if present in the theory.

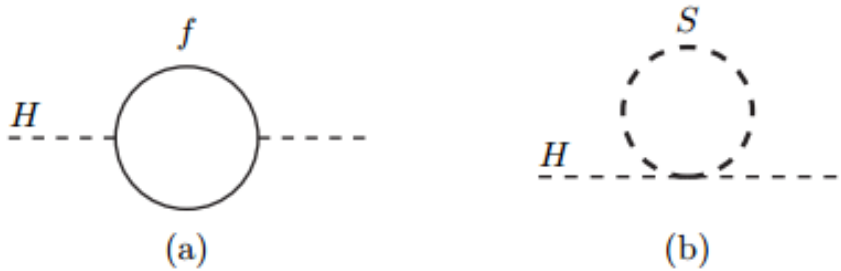

(a) (b)

Figure 1.1: One-loop quantum corrections to the Higgs squared mass parameter m_H^2, due to (a) a Dirac fermion f, and (b) a scalar S.

Contribution from (a) and (b):

$$m_H^2 = \frac{-|\lambda_f|^2 \Lambda_{UV}^2}{8\pi^2} \tag{4}$$

$$m_H^2 = \frac{\lambda_S}{16\pi^2}[\Lambda_{UV}^2 - 2m_S^2 \log(\frac{\Lambda_{UV}}{m_S})] \tag{5}$$

Choice of $\lambda_S = |\lambda_f|^2$ cancels the divergent contribution to higgs mass.

Contribution to the light Majorana neutrino mass

- Active neutrinos have masses $m_\nu \simeq \frac{y_\nu^2 v_u^2}{M_R}$, as in Type 1 seesaw mechanism. For $M_R \sim \mathcal{O}(100)\,GeV$, $y_\nu = 10^{-6} - 10^{-7}$ to fit $m_\nu \sim \mathcal{O}(0.1)$eV.
- Radiative corrections to neutrinos from sneutrino-neutralino loops in presence of left-right sneutrino mixing.
- Contribution proportional to mass splitting between CP even and CP odd sneutrino, i.e, B_M parameter for significant L-R mixing controlled by T_ν. (Y.Grossman, et. al, hep-ph/9702421)

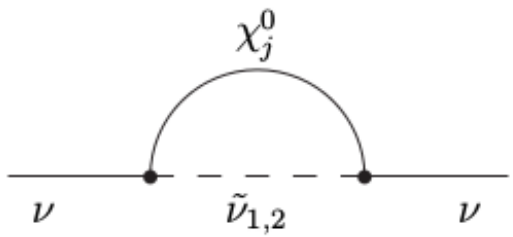

Figure: Schematic diagram showing the leading one-loop contribution to the light neutrino mass.

- The radiative contribution to neutrino mass arising from $\widetilde{\chi}_i^0$-$\widetilde{\nu}$ loop is:

$$m_\nu^{(1)} = \frac{g^2 \Delta m_{\widetilde{\nu}}}{32\pi^2 cos^2\theta_W} \Sigma_j f(y_j) |Z_{jZ}|^2 \tag{6}$$

$$\text{where } f(y_j) = \sqrt{y_j} \frac{[y_j - 1 - ln(y_j)]}{(1-y_j)^2},\ y_j = \frac{m^2_{\widetilde{\nu}}}{m^2_{\widetilde{\chi}_j^0}},$$

$$Z_{jZ} = Z_{j2} cos\theta_W - Z_{j1} sin\theta_W .$$

Electroweak Naturalness

After electroweak symmetry breaking,

$$\frac{M_Z^2}{2} = \frac{m_{H_d}^2 - (m_{H_u}^2)\tan\beta^2}{\tan\beta^2 - 1} - \mu^2, \tag{7}$$

where $m_{H_d}^2$ and $m_{H_u}^2$ are the soft squared mass matrix for up and down type Higgs doublets.

- Electroweak scale fine tuning Δ_{EW} (Baer, et. al, arXiv: 1306.2926) as a measure of naturalness, i.e $\mu <= 300$ GeV, $\Delta_{EW} \leq 30$.

$$\Delta_{EW} = \frac{max(|\frac{-m_{H_u}^2 \tan^2\beta}{\tan^2\beta - 1}|, ..., |-\mu^2|)}{M_Z^2/2}$$

- Focus on low μ parameter values and hence a light higgsino sector.
- Stops and gluinos may be kept heavy upto 1.5 and 3-4 TeV respectively.

Simulation details

- SUSY Signal: $\widetilde{\chi}_1^+\widetilde{\chi}_1^-$, $\widetilde{\chi}_2^0\widetilde{\chi}_1^0$, $\widetilde{\chi}_1^0\widetilde{\chi}_1^\pm$, $\widetilde{\chi}_2^0\widetilde{\chi}_1^\pm$
- UFO file from SARAH
- Spectrum Generator: SARAH-SPheno
- Madgraph5 $\rightarrow$ Pythia6 $\rightarrow$ Delphes-v3 for event generation,showering and detector simulation.
- MLM matching performed for SM background with QCUT values 20 GeV.
- Benchmarks passed through Checkmate and Madanalysis5 for constraints from recent LHC search results with low hadronic activity.

Primary Selection Cuts and Kinematic Observables

- We select leptons (e, μ) satisfying $p_T > 10$ GeV and $|\eta| < 2.5$.
- We choose photons with $p_T > 10$ GeV and $|\eta| < 2.5$.
- Reconstructed jets are identified as signal jets if they have $p_T > 40$ GeV and $|\eta| < 2.5$.
- Reconstructed b-tagged jets are identified with $p_T >$40 GeV and $|\eta| < 2.5$.
- Jets and leptons are isolated such that $\Delta R_{lj} > 0.4$ and $\Delta R_{ll} > 0.2$.

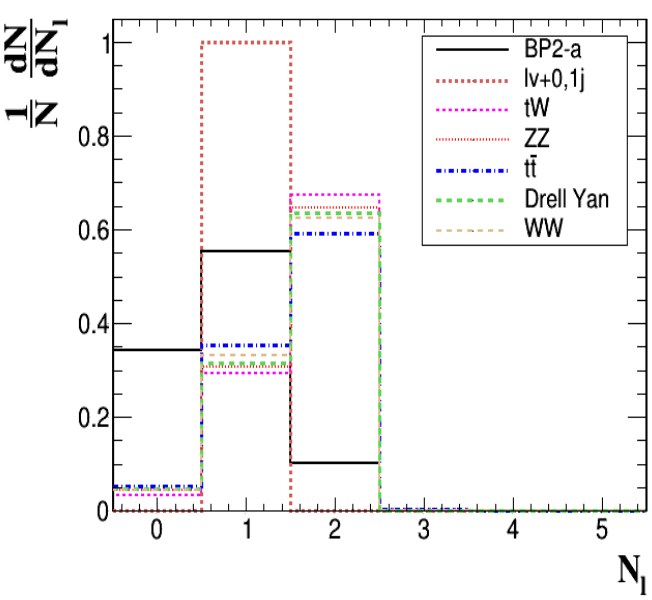

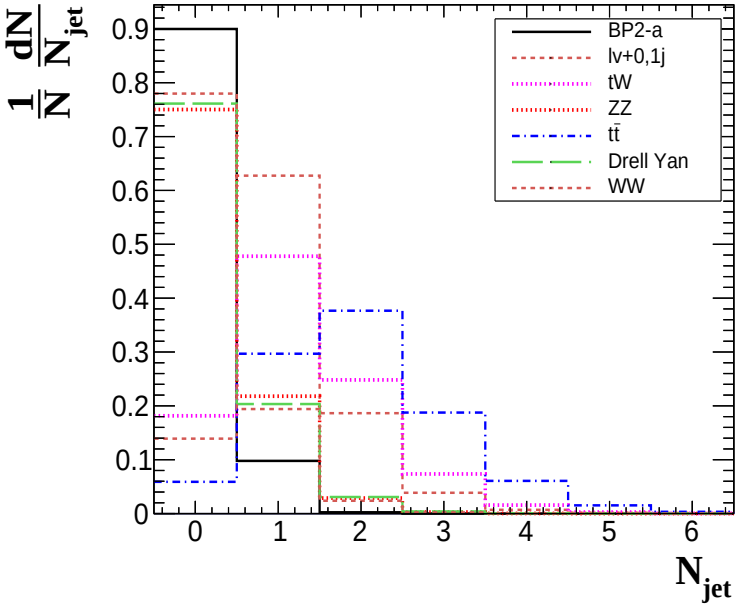

Figure: Normalized distributions for lepton and jet multiplicity for benchmark **BP2** and dominant SM backgrounds channels. respectively.

Focus on low hadronic activity to reduce SM backgrounds.

Important kinematic variable for monolepton final state

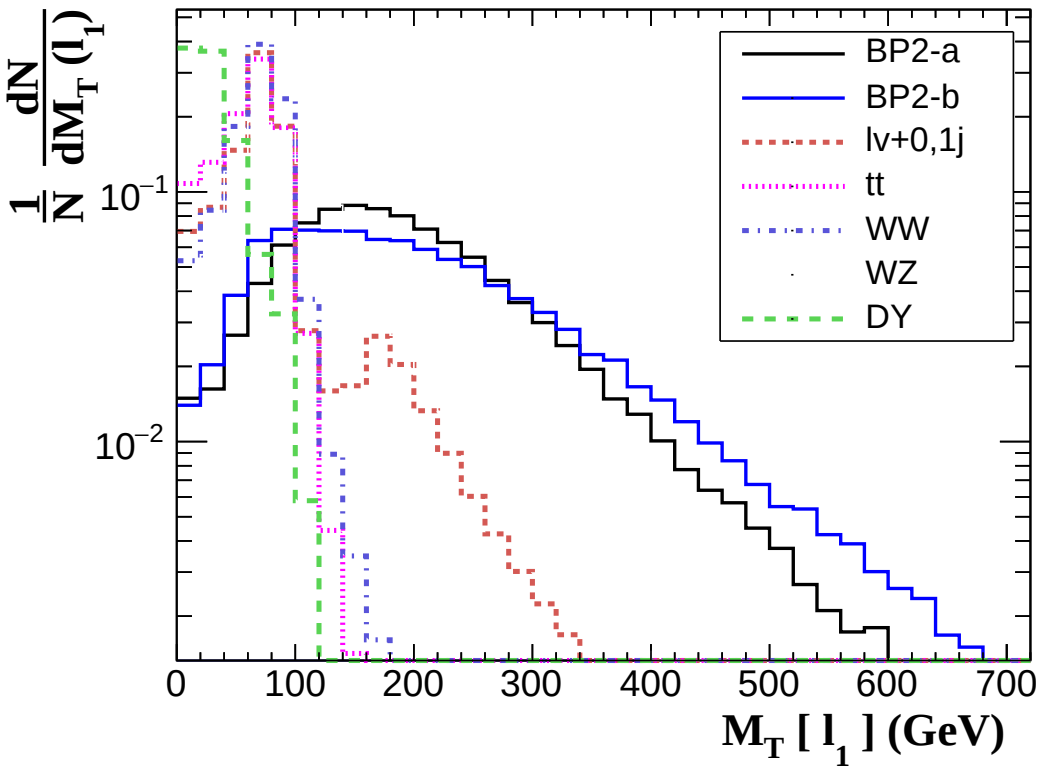

Figure: Normalized distribution for $M_T(l_1) = M_T(l, \not{E}_T) = \sqrt{2p_T(l)\not{E}_T(1-\cos(\Delta\phi))}$, the transverse mass of the leading lepton for SUSY signal **BP2 – a** and **BP2 – b** against the dominant SM backgrounds after selection of the mono-lepton final state.

Required Luminosities for Mono-lepton Channel

Signal	$\mathcal{L}_{3\sigma}$ (fb^{-1})	$\mathcal{L}_{5\sigma}$(fb^{-1})
BP1	254	704
BP2-a	1384	3485
BP2-b	106	293
BP3	613	1701
BP4	448	1245

Table: Required luminosities for discovery of mono lepton final states with missing energy at $\sqrt{s} = 13$ TeV LHC.

Monolepton channel is a good probe for this scenario for most benchmarks. Also pointed out earlier by Kraml, et. al (1503.02960).

Important Kinematic variables for OSDL final state

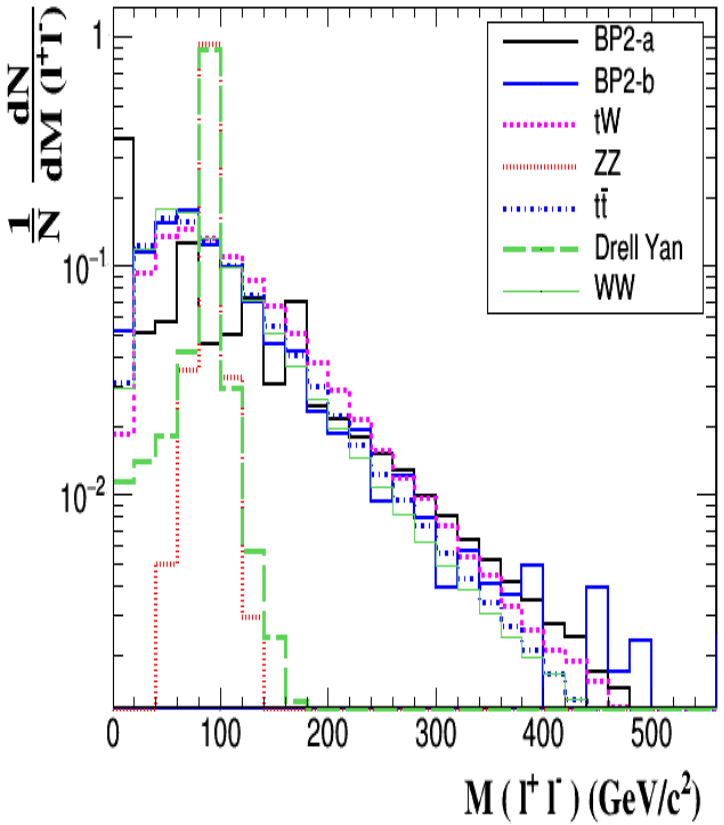

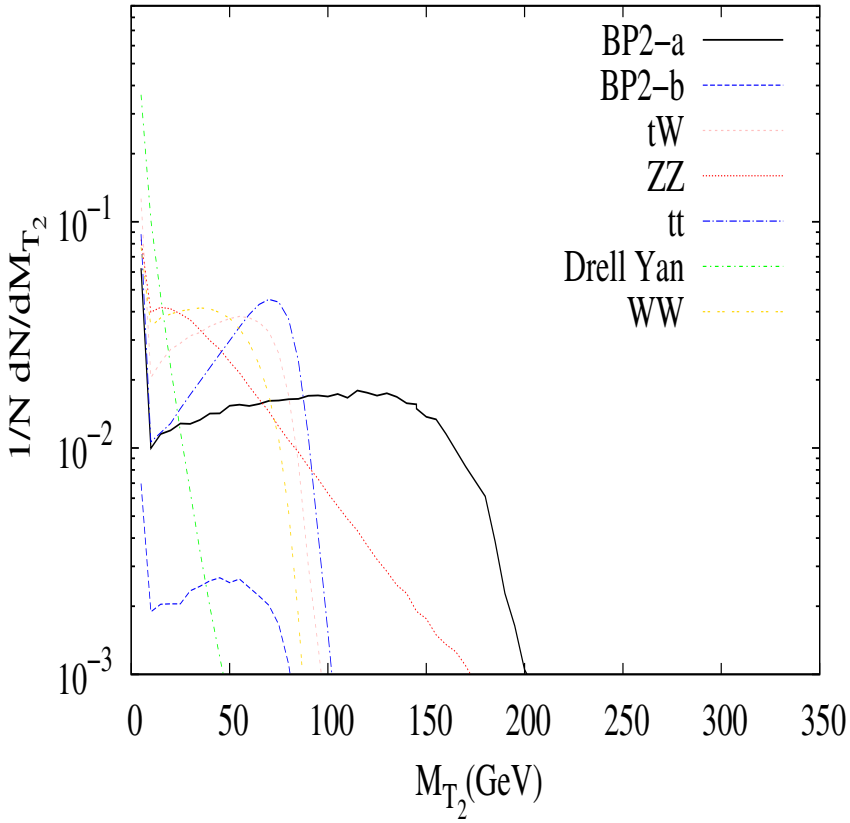

Figure: Normalized distributions of several kinematic variables after selecting the final state with two opposite sign leptons.

Required Luminosities for OSDL channel

Signal	$\mathcal{L}_{3\sigma}$ (fb^{-1})	$\mathcal{L}_{5\sigma}$(fb^{-1})
BP1	568	1576
BP2-a	51	142
BP2-b	1.83×10^4	5.07×10^4
BP3	1035	2875
BP4	160	444

Table: Required luminosities for discovery of opposite sign di-lepton + $\not{E}_T$ final states at $\sqrt{s} = 13$ TeV LHC.

Most favoured channel for large leptonic branching fractions and large mass gap scenarios ($\mathbf{BP2-a}$) whereas suppressed for more compressed scenarios where mono-lepton is a better probe.

Required Luminosities for SSDL channel

Signal	$\mathcal{L}_{3\sigma}$ (fb^{-1})	$\mathcal{L}_{5\sigma}$(fb^{-1})
BP2-b	811	2251
BP4	1052	3845

Table: Required luminosities for discovery of same sign di-lepton final states with missing energy at $\sqrt{s} = 13$ TeV LHC.

Favoured for channels with $\widetilde{\chi}_1^{\pm}$ as NLSP however strongly constrained from current searches. For $\mu = 300$ GeV, SSDL branching $\leq 4\%$ at most. For higher $\mu = 400$ GeV, Br $= 10\%$ but luminosity increases owing to a reduced production cross-section. Still a strong confirmatory channel for discovery.

Monolepton + $\leq 1j + \not{E}_T$

Dominant backgrounds come from:

- $l^{\pm}\nu$+0,1 jets (including contributions from both on-shell and off-shell W boson),
- $t\bar{t}$ (where one of the top quark decays hadronically and the other semi-leptonically).
- Single top quark production ($t(\bar{t})j,\ tW$).
- W^+W^-+ jets ($W \to l\nu$, $W \to jj$).
- $t\bar{t}W$+ jets (when both top quarks decay hadronically and $W \to l\nu$) and
- WZ (with $W \to l\nu$, $Z \to \nu\bar{\nu}/jj$).

Other subdominant contributions come from $t\bar{t}$ (where both top quarks decaying semi-leptonically), Drell Yan process ($l^+l^- + 0, 1j$) and ZZ, ($Z \to l^+l^-, Z \to \nu\bar{\nu}/jj$) from misidentification.

Kinematic Cuts used

- **M1:** $N_l = 1$, $p_T(l_1) > 25$ **GeV.**
- **M2:** $M_T(l_1) > 150$ **GeV.**
- **M3:** $N_b = 0$
- **M4:** $N_j <= 3$
- **M5:** $\not{E}_T > 100$ **GeV.**
- **M6:** $N_j <= 1$

Opposite sign dileptons + 0j + $\not{E}_T$

Dominant SM contributions to the opposite sign di-lepton signal with missing energy come from:

- $t\bar{t}$
- tW
- Drell Yan
- W^+W^- $(W^+ \to l^+\nu, W^- \to l^-\bar{\nu})$
- ZZ ($Z \to l^+l^-, Z \to jj/\nu\bar{\nu}$)
- WZ+jets $(W \to jj, Z \to l^+l^-)$

Kinematic cuts used

- **D1:** $N_l = 2$ **(opposite sign),** $N_\gamma = 0$
- **D2:** $p_T(l_1) > 20$ **GeV,** $p_T(l_2) > 10$ **GeV**
- **D3:** $M_{l^+l^-} > 10$**,** $M(l^+l^-)$ **outside the Z window(**$[76 : 106]$**)**
- **D4:** $N_b = 0$
- **D5:** $N_j = 0$
- **D6:** $\not{E}_T > 80$ **GeV**
- **D7:** $M_{T_2} > 90$ **GeV**
- **D8:** $\not{E}_T > 100$ **GeV**

Same-sign dilepton + 0 j+$\not{E}_T$

Dominant sources of SM backgrounds :

- WZ
- ZZ
- $W^{\pm}W^{\pm} + jj$
- $t\bar{t}W$
- $t\bar{t}Z$
- WWW

Kinematic cuts used:

- **S1:** $N_l = 2$ **(SS),** $p_T(l_1) > 20$ **GeV,** $p_T(l_2) > 15$ **GeV,** $N_b = 0$
- **S2:** $M_T(l_1) > 100$ **GeV**
- **S3:** $N_j <= 2$
- **S4:** $\not{E}_T > 100$ **GeV**
- **S5:** $N_j = 0$

Relevant current searches at LHC

Final State	ATLAS	CMS
1 l + $\not{E}_T$	1706.4786	CMS-PAS-SUS-16-052
2 l + $\not{E}_T$	ATLAS-CONF-2017-039	CMS-PAS-SUS-17-009(2)
2 same-sign leptons + $\not{E}_T$	-	CMS-SUS-16-039

Table: Leptonic searches at $\sqrt{s} = 13$ TeV LHC with few jets (i,e, $N_j \leq 2$), as relevant for this study.

Forecast from current searches

		Luminosity (in fb^{-1}) for 3σ				
	Ref.	**BP1**	**BP2-a**	**BP2-b**	**BP3**	**BP4**
$l^{\pm}l^{\mp}$+ 0 jet+ $\not{E}_T$	ATLAS-CONF-2017-039	13397	812	-	-	958
$l^{\pm}l^{\mp}$+ 0 jet+ $\not{E}_T$	ATLAS-CONF-2017-039	2191	162	-	-	104
$l^{\pm}l^{\mp}$ + 0 jet+$\not{E}_T$	CMS-PAS-SUS-17-009	-	2223	-	-	385
$l^{\pm}l^{\pm}$ + 0 jet+ $\not{E}_T$	CMS-SUS-16-039	-	-	1997	-	2726
$l^{\pm}l^{\pm}$ + 1 jet+ $\not{E}_T$	CMS-SUS-16-039	-	-	4039	-	4901

Table: Forecast for luminosity for 3σ excess using present experimental searches using 36 fb^{-1} of data at LHC. The blank spaces indicate that the benchmark is not sensitive to the final state analysis. We do not show the forecast from current monoleptonic searches as it gives much weaker sensitivity to our scenario.

Monolepton $+ \leq 1j + \not{E}_T$

	Number of events after cut					
	M1	**M2**	**M3**	**M4**	**M5**	**M6**
BP1	2543	1987	1946	1936	1601	1429
BP2-a	1495	944	922	916	706	611
BP2-b	6252	3194	3128	3118	2462	2215
BP3	1.06×10^4	1664	1614	1601	1138	919
BP4	3919	1793	1751	1740	1258	1074
SM BKG						5.74×10^5

Table: Mono-lepton + missing energy signal final state number of events at 100 fb^{-1} for SUSY signals.

Monolepton $+ \leq 1j + \not{E}_T$

	Number of events after cut					
	M1	**M2**	**M3**	**M4**	**M5**	**M6**
BP1	2543	1987	1946	1936	1601	1429
BP2-a	1495	944	922	916	706	611
BP2-b	6252	3194	3128	3118	2462	2215
BP3	1.06×10^4	1664	1614	1601	1138	919
BP4	3919	1793	1751	1740	1258	1074
SM BKG						5.74×10^5

Table: Mono-lepton + missing energy signal final state number of events at 100 fb^{-1} for SUSY signals.

Background Cut Flow

Background	Number of events after cut					
	M1	**M2**	**M3**	**M4**	**M5**	**M6**
$l\nu + 0, 1j$	1.07×10^7	1.09×10^6	1.08×10^6	1.08×10^5	5.77×10^5	5.49×10^5
Drell Yan	3.52×10^7	3.47×10^4	3.34×10^4	5991	5272	3674
WW	8.04×10^5	5696	5485	5446	1329	1130
WZ	1.56×10^5	2.54×10^4	2.48×10^4	2.20×10^4	1.55×10^4	11523
ZZ	4938	912	900	899	551	492
$t\bar{t}$	2.04×10^6	5.97×10^4	1.79×10^4	1.68×10^4	1.17×10^4	6399
Single top	3.68×10^6	2.05×10^4	8517	8088	2659	1603
Total						5.74×10^5

Table: Mono−lepton + missing energy signal final state number of events at 100 fb^{-1} for SM background.

Opposite-sign dileptons + 0 j + $\not{E}_T$

Signal	Number of events after cut						
	D1	**D2**	**D3**	**D4**	**D5**	**D7**	**D8**
BP1	130	129	112	109	68	22	21
BP2-a	306	271	265	161	108	76	72
BP4	209	298	246	241	153	81	40

Signal	Number of events after cut						
	D1	**D2**	**D3**	**D4**	**D5**	**D6**	
BP2-b	455	452	351	345	230	45	
BP3	2424	2394	1840	1805	1186	189	
Total Bkg						41009	271

Table: Opposite Sign di-lepton + $\not{E}_T$ final state number of events at 100 fb^{-1} for SUSY signals.

	No. of events							
	D1	**D2**	**D3**	**D4**	**D5**	**D6**	**D7**	**D**
DY	1.2×10^8	1.1×10^8	8.9×10^6	8.8×10^6	6.9×10^6	506	293	5
W^+W^-	1.44×10^5	1.4×10^5	1.1×10^5	1.1×10^5	1×10^5	5813	24	1
ZZ	1.7×10^4	1.7×10^4	656	651	504	117	50	4
WZ	6×10^4	6×10^4	5399	5208	1554	92	6	
$t\bar{t}$	6.2×10^5	6.2×10^5	4.9×10^5	1.5×10^5	3.5×10^4	2.6×10^4	132	1
tW	1.8×10^5	1.7×10^5	1.4×10^5	6.8×10^4	3×10^4	8181	114	5
Total						41009		2

Table: Opposite Sign di-lepton + $\not{E}_T$ final state number of events at 100 fb^{-1} for Standard Model backgrounds.

Signal	Number of events after cut:				
	S1	**S2**	**S3**	**S4**	**S5**
BP1	5	5	5	4	2
BP2-a	3	2.5	2.3	1.6	1
BP2-b	32	23	22	15	8
BP3	2	0.5	0.5	0.2	0.1
BP4	30	23	23	13	7
Total background					55

Table: Same sign di-lepton + $\not{E}_T$ final state number of events at 100 fb^{-1} for SUSY signals.

SSDL Background Cut flow

SM Backgrounds	Number of events after cut				
	S1	**S2**	**S3**	**S4**	**S5**
WZ	3856	1053	930	194	39
ZZ	94	6	5	0.5	0.2
WWW	60	29	21	7	0.6
W^+W^+jj	416	175	116	56	2
W^-W^-jj	188	82	57	18	0.5
tW	40	20	19	7	4
$t\bar{t}W$	128	60	30	13	1
$t\bar{t}$	90	65	50	28	8
Total background					55

Table: Same sign di-lepton + $\not{E}_T$ final state number of events at 100 fb^{-1} for SM background.

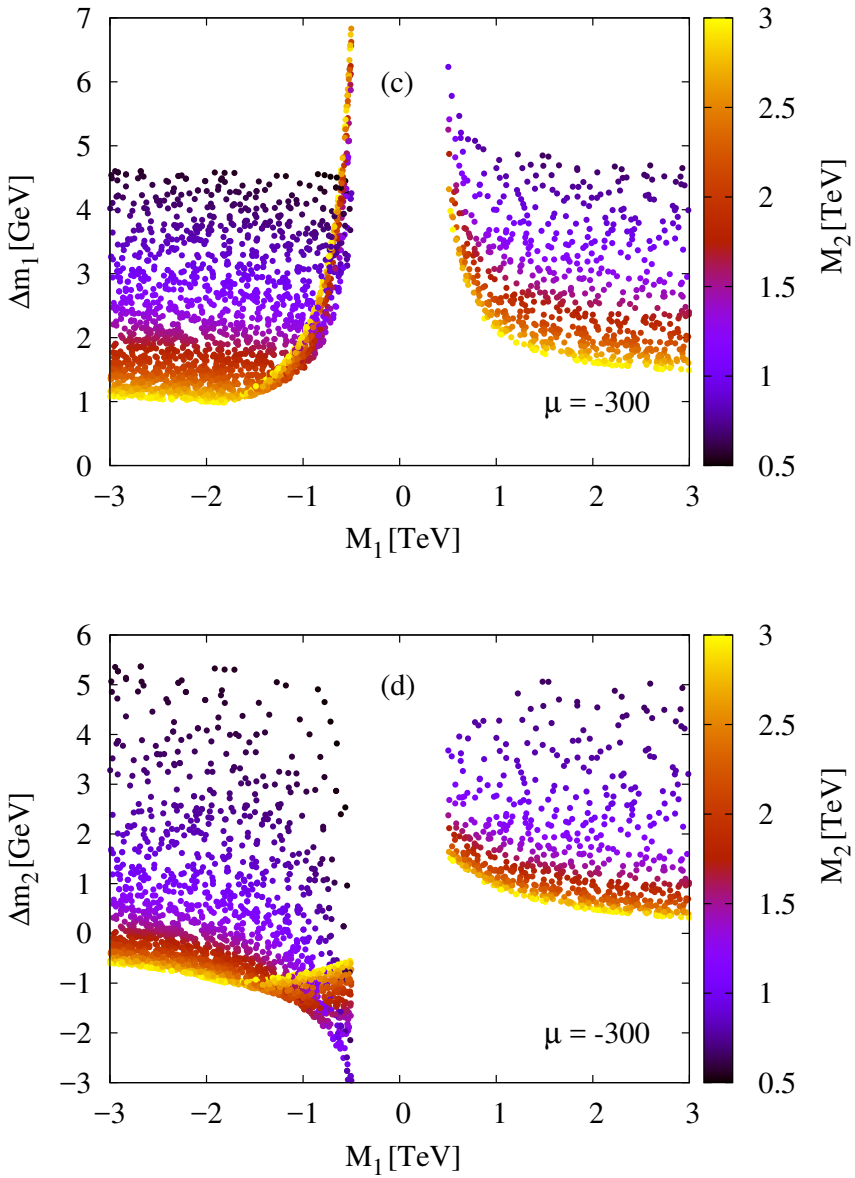

Figure: The left (right) panel shows the variation of the mass difference $\Delta m_1 = m_{\tilde{\chi}^+_1} - m_{\tilde{\chi}^0_1}$ ($\Delta m_2 = m_{\tilde{\chi}^0_2} - m_{\tilde{\chi}^+_1}$) between $\tilde{\chi}^\pm_1$ and $\tilde{\chi}^0_1$ [$\tilde{\chi}^0_2$] for

Leptonic Branching of the Higgsinos

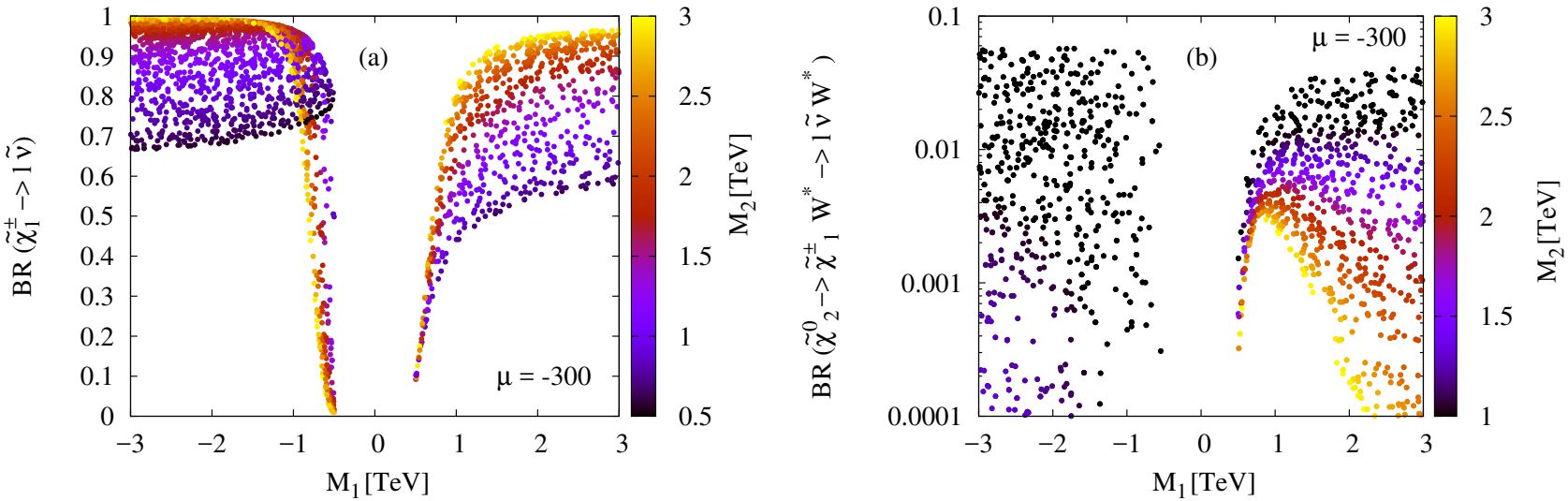

Figure: Variation of the leptonic branching ratios of $\widetilde{\chi}_1^{\pm} \to l\widetilde{\nu}$ and $\widetilde{\chi}_2^0 \to l\widetilde{\nu}W^*$ against the bino soft mass parameter, M_1 for the Higgsino mass parameter, $\mu = -300$ GeV. The wino mass parameter M_2 is indicated in the palette.

Limits on light higgsinos

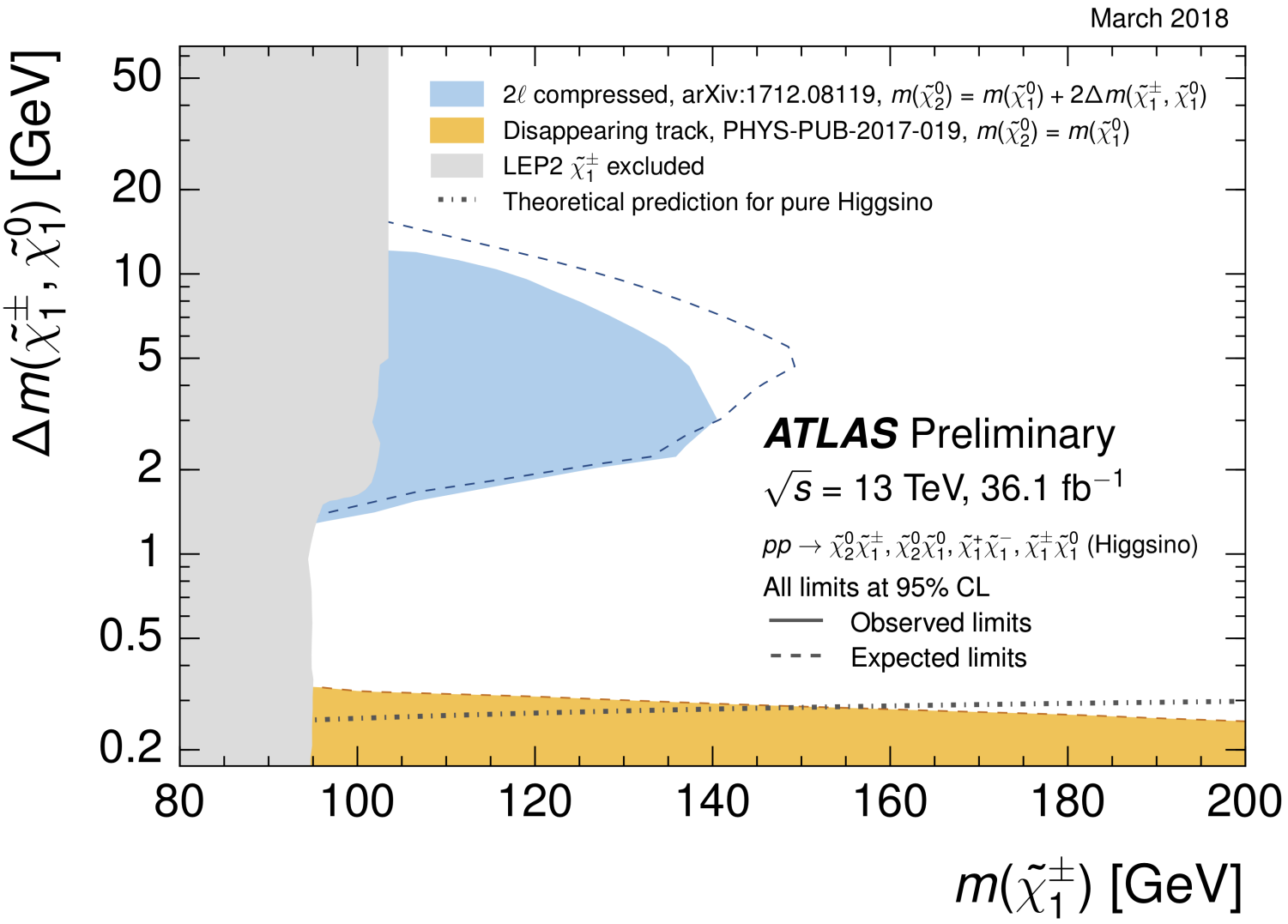

Decay rates to Gravitino

$$\Gamma\left(\widetilde{\chi}_1^0 \to \gamma\widetilde{G}\right) \propto |N_{11}cos\theta_W + N_{12}sin\theta_W|^2$$

$$\Gamma\left(\widetilde{\chi}_1^0 \to Z\widetilde{G}\right) \propto \left(|N_{11}sin\theta_W - N_{12}cos\theta_W|^2 + \frac{1}{2}|N_{14}cos\beta - N_{13}sin\beta|^2\right)$$

$$\Gamma\left(\widetilde{\chi}_1^0 \to h\widetilde{G}\right) \propto |N_{14}sin\alpha - N_{13}cos\alpha|^2$$